

# Neural Nonmyopic Bayesian Optimization in Dynamic Cost Settings

Sang T. Truong<sup>1</sup>, Duc Q. Nguyen<sup>2</sup>, Willie Neiswanger<sup>3</sup>, Ryan-Rhys Griffiths<sup>4</sup>,  
Stefano Ermon<sup>1</sup>, Nick Haber<sup>1</sup>, Sanmi Koyejo<sup>1</sup>

<sup>1</sup>Stanford University, <sup>2</sup>National University of Singapore,

<sup>3</sup>University of Southern California, <sup>4</sup>FutureHouse, Inc.

## Abstract

Bayesian optimization (BO) is a common framework for optimizing black-box functions, yet most existing methods assume static query costs and rely on myopic acquisition strategies. We introduce LookaHES, a nonmyopic BO framework designed for dynamic, history-dependent cost environments, where evaluation costs vary with prior actions, such as travel distance in spatial tasks or edit distance in sequence design. LookaHES combines a multi-step variant of  $H$ -Entropy Search with pathwise sampling and neural policy optimization, enabling long-horizon planning beyond twenty steps without the exponential complexity of existing nonmyopic methods. The key innovation is the integration of neural policies, including large language models, to effectively navigate structured, combinatorial action spaces such as protein sequences. These policies amortize lookahead planning and can be integrated with domain-specific constraints during rollout. Empirically, LookaHES outperforms strong myopic and nonmyopic baselines across nine synthetic benchmarks from two to eight dimensions and two real-world tasks: geospatial optimization using NASA night-light imagery and protein sequence design with constrained token-level edits. In short, LookaHES provides a general, scalable, and cost-aware solution for robust long-horizon optimization in complex decision spaces, which makes it a useful tool for researchers in machine learning, statistics, and applied domains. Our implementation is available at <https://github.com/sangttruong/nonmyopia>.

## 1 Introduction

Bayesian optimization (BO) combines a probabilistic surrogate model, often a Gaussian process (GP), with an acquisition function to guide the search on black-box functions [Shahriari et al., 2016, Frazier, 2018, Garnett, 2022]. Standard BO typically assumes static query costs [Kushner, 1962, Kushner, 1964], but this assumption does not always practically hold. In many applications, these costs vary with prior actions. For example, in geological surveys, the cost of sampling a site depends on its distance from previous sites, reflecting transportation expenses [Bordas et al., 2020]. In biological sequence design, making a single token edit is inexpensive, whereas larger edits that move beyond a small edit distance are far more costly [Guo et al., 2004, Błażej et al., 2017]. Such environments introduce dynamic, history-dependent cost structures, where the cost of evaluating a point depends on the most recent query or even the full query trajectory [Aglietti et al., 2021, Lee et al., 2021, Folch et al., 2022, Folch et al., 2024]. Accounting for these costs fundamentally changes the optimization problem: the feasible decision space evolves with history, and effective strategies must plan over multiple steps rather than rely on purely myopic choices.

As cost structures become more complex and interdependent, myopic strategies fail to capture long-term benefits, highlighting the need for nonmyopic BO. Nonmyopic BO incorporates lookahead steps to improve current decision [González et al., 2016, Astudillo et al., 2021, Yue and Kontar, 2020, Jiang et al., 2020a]. A natural way to formalize this problem is as a Markov Decision Process (MDP), which is commonly used in sequential decision-making [Garcia and Rachelson, 2013, Puterman, 2014]. To determine the optimal next action in a sample-efficient manner, an MDP frames the decision process as a cost-constrained model-based reinforcement learning (CMBRL) problem, where the queried inputs are states and actions influence the transitions between consecutive states.

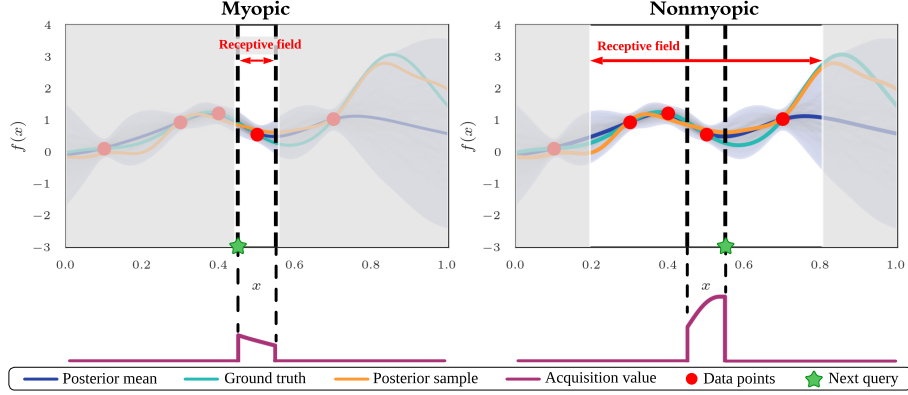


Figure 1: Comparison of myopic and nonmyopic BO in a dynamic cost setting. The unshaded region denotes the current receptive field, i.e., the subset of the input space considered for the next query. Myopic BO (left) has a narrow receptive field, focusing only on immediate reward. Nonmyopic BO (right) expands the receptive field by accounting for future queries, enabling selection of points that may appear suboptimal in the short term but lead to higher long-term rewards (see acquisition values in the bottom row). This broader planning horizon allows the decision-maker to access high-reward regions that greedy strategies cannot reach. See Section 3.3 for details.

However, CMBRL exhibits two critical mismatches with nonmyopic BO. First, its reliance on simple neural network policies limits scalability to large, structured action spaces, as in biological sequence design, where edits carry semantic meaning and domain constraints [Janner et al., 2019, Wang and Ba, 2020, Hafner et al., 2021, Stolze et al., 2015, Hamed et al., 2024]. Integrating pre-trained large language models (LLMs) as policies can exploit such structure, yet most existing reinforcement learning frameworks target single-step or contextual bandit regimes rather than multi-step nonmyopic BO [Palo et al., 2023, Zhuang et al., 2024, Hazra et al., 2024, Ouyang et al., 2024, von Werra et al., 2020, Hu et al., 2025, Zheng et al., 2024, Harper et al., 2019]. Secondly, in domains requiring nonmyopic planning such as sequence editing, state transitions are often deterministic, reducing the need for stochastic world models [Janner et al., 2019, Hafner et al., 2021, Wang and Ba, 2020]. Moreover, CMBRL typically integrates neural reward models, which causes it to struggle to represent reward uncertainty, which is important for balancing exploration-exploitation [Treven et al., 2024, Sun et al., 2024, Zangirolami and Borrotti, 2024, Ez-zizi et al., 2023]. These reward models are often miscalibrated, yielding overconfident or underconfident estimates and, consequently, leading to suboptimal actions [Minderer et al., 2021, Zhao et al., 2024, Sun et al., 2024]. Explicitly modeling aleatoric and epistemic uncertainty via acquisition functions improves robustness to dynamic, noisy settings such as wet-lab biological testing,

where small errors can noticeably change outcomes [Lötjens et al., 2019, Luis et al., 2023, Ez-zizi et al., 2023, Caraus et al., 2015].

Recent advances in nonmyopic BO have achieved notable progress. While nonmyopic BO has been studied for decades, traditional methods can scale only up to a four-step lookahead [Snoek et al., 2012, Wu and Frazier, 2019, Astudillo et al., 2021, Jiang et al., 2020b, Lee et al., 2021] and typically ignore cost models. These approaches rely on free variables, leading to exponential complexity as the lookahead horizon increases. More recent work has sought to incorporate dynamic costs [Ling et al., 2016, Liu et al., 2023], yet these methods still suffer from an exponential growth in optimization parameters. Neural policies, including transformer-based models, have shown promise by variationally optimizing the decision variables, thereby reducing the number of optimization parameters [Maraval et al., 2023, Nwankwo and Bindel, 2024, Cheon et al., 2025]. However, these approaches still require an exponential number of rollout trajectories during lookahead. A promising direction to alleviate this is decomposing actions into micro-actions, which approximates long-horizon lookahead with finer-grained steps [Kharkovskii et al., 2020]. Nevertheless, splitting into macro-actions is less effective, as it inflates the action space, hinders correlation modeling, and reduces adaptivity without new observations.

To address these limitations, we introduce LookaHES, a cost-constrained nonmyopic BO algorithm. LookaHES reduces the exponential complexity of multi-step optimization by combining a multi-step variant of  $H$ -

Entropy Search with pathwise sampling and neural policy optimization. Our approach balances exploration and exploitation using a Bayesian reward model and scales to horizons of twenty or more steps, well beyond the four-step limits of prior work. Additionally, LookaHES can be applied across diverse domains, from sequence design to natural language processing, where multiple interactions are required before a final decision is made. Our contributions are stated as follows.

- We formulate nonmyopic BO in dynamic cost settings with cost models inspired by real-world scenarios such as protein sequence design.
- We employ a neural policy to variationally optimize all decision variables (i.e., reduce the number of optimization parameters) and pathwise sampling to reduce trajectory samples, enabling long-horizon planning and effective handling of large structured combinatorial action spaces.
- We evaluate LookaHES on nine synthetic benchmarks (2D–8D, varying noise) and a real-world geospatial optimization task using NASA night-light imagery, showing consistent improvements over myopic and nonmyopic baselines.
- We demonstrate the effectiveness of LookaHES on a constrained protein sequence design task, where combinatorial complexity hampers traditional BO. Leveraging a LLaMa-3.2-based policy, our method exploits pretrained domain knowledge to guide edits, achieving superior performance.

## 2 Related Works

We review related work on cost-sensitive BO by introducing a taxonomy that classifies costs into four categories based on their uncertainty (known vs. unknown) and variability (static vs. dynamic), as summarized in Table 1. Within static costs, prior work distinguishes between homogeneous costs, where all queries incur the same expense, and heterogeneous costs, where the cost depends on the specific query. To illustrate the distinction between cost structures, we visualize the uncertainty and variability of these structures as probabilistic graphical diagrams in Figure 6. Additional related works are provided in Appendix B.

Prior work has considered unknown heterogeneous costs, particularly in hyperparameter optimization, where costs are static but configuration-dependent [Astudillo et al., 2021, Lee et al., 2021, Luong et al., 2021, Snoek et al., 2012]. Other approaches assume constant, known costs across the search space [Wu and Frazier, 2019,

Nyikosa et al., 2018, Lam et al., 2016], thereby ignoring cost variability. In contrast, our study addresses Bayesian optimization with known, dynamic costs, a regime not much explored in earlier work. For instance, [Liu et al., 2023, Ling et al., 2016] introduce Euclidean cost-constrained lookahead acquisition functions related to our setting. However, these methods fail to overcome the exponential growth in decision variables and rollout trajectories, limiting their scalability to long horizons. Our proposed LookaHES mitigates these limitations by employing a language-model-based policy to reduce the number of optimization parameters and pathwise sampling to control the number of rollout trajectories.

## 3 Method

### 3.1 Problem Setup

The decision maker (DM) aims to optimize a black-box function  $f: \mathcal{X} \rightarrow \mathcal{Y}$ , with  $\mathcal{Y} \subseteq \mathbb{R}$ , by sequentially issuing  $T$  queries. At each step  $t \in \{1, \dots, T\}$ , the DM selects a query  $x_t \in \mathcal{X}$  and observes a noisy evaluation  $y_t = f(x_t) + \epsilon_t$ . The complete history of queries and observations is denoted by  $x_{1:T} = [x_1, \dots, x_T]$  and  $y_{1:T} = [y_1, \dots, y_T]$ , respectively. Given a prior distribution over the parameters  $p(\theta)$ , a surrogate model  $f_\theta$  of the black-box function  $f^*$  is sampled by  $\theta \sim p(\theta)$ . At time step  $t$ , given the history of queries and observations, the function parameters' posterior distribution is  $p_t(\theta) = p(\theta|D_t) = p(\theta|x_1, y_1, \dots, x_t, y_t)$ .

After  $T$  queries, DM selects an action  $a \in \mathcal{A}$ . In general Bayesian decision-making literature,  $\mathcal{A}$  can be distinct from  $\mathcal{X}$ . For example, the DM might query the black box function to find the top- $k$  or level set. This paper focuses on global optimization; hence, the action set is the same as the query set,  $\mathcal{A} = \mathcal{X}$ <sup>1</sup>. The loss function is given by  $\ell(f^*, a) = -f^*(a)$ . Following prior work [Russo and Van Roy, 2016, Kandasamy et al., 2018], the Bayesian cumulative regret at timestep  $T$  is defined as  $\mathbb{E} \left[ \sum_{t=1}^T (f^*(a^*) - f^*(a_t)) \right]$ , where the expectation is taken over the randomness from the environment, the sequence of queries, and the final actions. We summarize our notations in Appendix A.

### 3.2 Decision-making Objective

The DM selects queries via an acquisition function. We consider  $H$ -Entropy Search (HES) [DeGroot, 1962,

<sup>1</sup>We still use the notion of a final action to maintain consistency with the literature. We note that our method can apply to a general action set, and studying that is beyond the scope of our paper.

Table 1: Classification of Cost Types Based on Uncertainty and Variability.

	Known Cost	Unknown Cost
Static	Costs remain constant regardless of the queries made during optimization. These costs are predictable and can be pre-determined, making them straightforward to budget and plan [Wu and Frazier, 2019, Nyikosa et al., 2018, Lam et al., 2016].	Costs are static but unpredictable due to external factors such as system fluctuations or resource availability. While they are static, their unpredictability complicates cost estimation [Astudillo et al., 2021, Lee et al., 2021, Snoek et al., 2012, Luong et al., 2021].
Dynamic	Costs change based on the sequence of previous queries. These costs depend on previous optimization steps but remain predictable, allowing for some level of planning [Liu et al., 2023, Ling et al., 2016].	Costs depend on prior queries and are unpredictable, often arising in variable environments like dynamic resource allocation or uncertain execution times, which are difficult to estimate in advance. To our knowledge, no prior work addresses this.

Neiswanger et al., 2022], a decision-theoretic entropy-based framework that generalizes common acquisition functions such as Knowledge Gradient [Frazier et al., 2009] and Expected Improvement [Šaltenis, 1971]. We focus on its multi-step lookahead variant, which accommodates dynamic cost structures  $c$ , and describe our procedure for optimizing a variational version of the acquisition function using a neural network policy.

For a prior  $p(f)$  and a dataset  $D_t = D_0 \cup \{(x_i, y_i)\}_{i=1}^t$ , the posterior  $\mathbb{H}_{\ell, c, \mathcal{A}}$ -entropy and the expected  $\mathbb{H}_{\ell, c, \mathcal{A}}$ -information gain (EHIG) at step  $t$  with loss function  $\ell$ , cost function  $c$ , action set  $\mathcal{A}$ , and Lagrange multiplier  $\lambda$ , and lookahead horizon  $L$  is

$$\begin{aligned} \mathbb{H}_{\ell, c, \mathcal{A}}[f|D_t] &= \inf_{a \in \mathcal{A}} \{\mathbb{E}_{p_t(f)}[\ell(f, a)] + \lambda c(x_{1:t}, a)\}, \\ \text{EHIG}_t(x_{1:L}) &= \mathbb{H}_{\ell, c, \mathcal{A}}[f|D_t] \\ &\quad - \mathbb{E}_{p_t(y_{1:L}|x_{1:L})} [\mathbb{H}_{\ell, c, \mathcal{A}}[f|D_{t+L}]]. \end{aligned}$$

Following the  $\mathbb{H}$ -information gain heuristics, the decision-maker selects the query  $x_{t+1} \in \mathcal{X}$  at each step  $t$  to maximize the expected  $\mathbb{H}$ -information gain:

$$\begin{aligned} x_{1:L}^* &= \arg \sup_{x_{1:L} \in \mathcal{X}^L} \text{EHIG}_t(x_{1:L}) \\ &= \arg \sup_{x_{1:L} \in \mathcal{X}^L} [-\mathbb{E}_{p_t(y_{1:L}|x_{1:L})} [\mathbb{H}_{\ell, c, \mathcal{A}}[f|D_{t+L}]]]. \end{aligned} \quad (1)$$

### 3.3 Dynamic Cost Bayesian Optimization

To model the dynamic cost, firstly, we define the cost of querying  $x_t$  as  $c(x_{<t}, x_t)$ , where  $c$  is an application-specific cost function provided to the decision-maker. The total cost to execute  $T$  queries is  $\sum_{t=1}^T c(x_{<t}, x_t)$ . We introduce two primary dynamic cost structures: (i) **Markovian cost**, which depends only on the previous query  $x_{t-1}$  and the current query  $x_t$ , typically based on the  $p$ -norm distance between them. Costs may be nonlinear, e.g., traveling within a radius  $r$  may be free, but beyond that, it grows at

a rate  $k$ , and observed costs may include noise  $\epsilon$ :  $c_{\text{Markov}}(x_{t-1}, x_t) = \max(k(\|x_t - x_{t-1}\|_p - r), 0) + \epsilon$ . Common instances include Euclidean cost ( $p = 2, r = 0$ ) as in ground surveys [Bordas et al., 2020], Manhattan cost ( $p = 1, r = 0$ ), and spotlight cost ( $k = \infty$ ), e.g., in biological sequence design where more than one token cannot be edited in a single experiment [Belanger et al., 2019]. (ii) **Non-Markovian cost**, which depends on the full query history, e.g., a traveler may receive a discount  $d$  if cumulative distance exceeds  $m$ , formalized as  $c_{\text{non-Markov}}(x_{<t}, x_t) = c_{\text{Markov}}(x_{t-1}, x_t) - d\mathbb{I}[\sum_{i=1}^{t-1} c_{\text{Markov}}(x_i, x_{i+1}) > m]$ . In practice, cost models can be learned from application data or designed by the decision maker. Under budget constraints, dynamic costs require nonmyopic planning to avoid high costs or local optima.

Importantly, under dynamic costs, **candidates in the query space  $\mathcal{X}$  are not equally considered** by the DM. For instance, in the spotlight cost, candidates outside the spotlight radius are effectively inaccessible. Looking ahead allows the DM to plan over future steps, considering candidates that may *become accessible after intermediate queries*. We define the decision receptive field as the subset of the input space considered by the DM. By looking ahead, the receptive field expands, allowing the DM to “invest” in suboptimal immediate queries if they enable better outcomes later, such as access to the global optimum (Figure 1). The longer the lookahead horizon is, the better the DMs plan their decision. Unfortunately, increasing the lookahead horizon leads to an exponential growth in decision variables and uncertainty, making planning intractable.

### 3.4 Neural Network Policy Optimization

In nonmyopic decision-making, the number of decision variables scales with the number of Monte Carlo (MC) rollout paths,  $p$ , and the horizon length,  $T$ . In the best-case scenario, where the number of MC samples

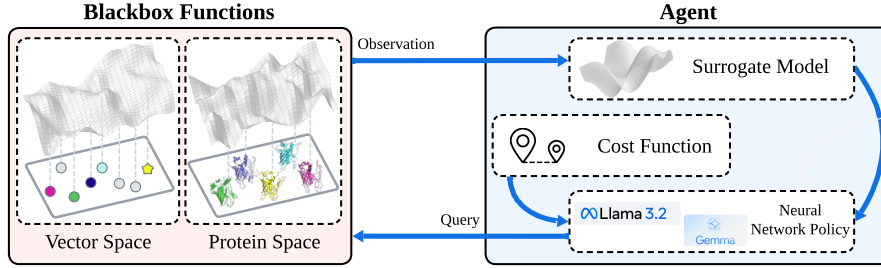


Figure 2: Process illustration. The black-box functions define complex objective landscapes in vector or protein spaces. The agent leverages a surrogate model to approximate the black-box function. The neural network policy generates the next queries to explore and exploit the optimization space. The query generation is guided by a dynamic cost function, ensuring efficient and targeted navigation of the search landscape.

grows linearly with the horizon, the policy complexity is  $\mathcal{O}(T)$ . In the worst case, the number of samples grows exponentially, leading to complexity  $\mathcal{O}(k^T)$ , where  $k$  is the number of samples per step. To mitigate this issue, we employ a neural network policy as it can reduce the number of optimization parameters to a constant with respect to the horizon. These policies have been widely applied in contexts such as policy gradient methods, variational autoencoders, and variational design of experiments [Schulman et al., 2017, Kingma and Welling, 2014, Foster et al., 2019].

From (1), we observe that for each lookahead step  $l \in [L]$ , the decision  $x_{t+l+1}$  is determined by the previous decision variables and corresponding observations,  $(x_{1:t+l}, y_{1:t+l})$ . This dependency can be modeled using a recurrent neural network (RNN) parameterized by  $\xi \in \Xi$ , which takes the history as input to predict the optimal next query:  $\xi : (x_{1:t}, y_{1:t}) \mapsto x_{t+1}$ . The corresponding posterior predictive  $y_{t+1}$  can then be computed by  $y_{t+1} \sim p_t(x_{t+1})$ . We maintain the gradients  $\frac{\partial \text{EHIG}_t(x_{1:L})}{\partial \xi}$  for optimizing  $x_{t+1}^* = \xi^*(x_{1:t}, y_{1:t})$  across the lookahead steps by applying the chain rule:

$$\frac{\partial \text{EHIG}_t(x_{1:L})}{\partial x_{t+L}} \frac{\partial x_{t+L}}{\partial \xi} + \frac{\partial \text{EHIG}_t(x_{1:L})}{\partial y_{t+L}} \frac{\partial y_{t+L}}{\partial x_{t+L}} \frac{\partial x_{t+L}}{\partial \xi}.$$

We can rewrite equation (1) as:

$$\begin{aligned} \xi^* = \arg \inf_{\xi \in \Xi} \mathbb{E}_{p_t(y_{1:L} | x_{1:L}, \xi)} & \left[ \inf_{a \in \mathcal{A}} \mathbb{E}_{p_{t+L}(f)} [\ell(f, a)] \right. \\ & \left. + \lambda c(x_{1:t}, x_{1:L}, a) \right]. \end{aligned} \quad (2)$$

In our experiments, the variational network is trained using fantasized data points. Specifically, when optimizing step  $t+1$ , we use the previously observed data points  $(x_{1:t}, y_{1:t})$  to generate lookahead data points  $(x_{t+1:t+L}, y_{t+1:t+L})$  through an autoregressive process:  $x_{t+l+1} = \xi_t(x_{1:t+l}, y_{1:t+l})$  and  $y_{t+l+1} \sim p_{t+l}(x_{1:t+l})$ . These fantasized data points are then used to compute the optimization objective and find the optimal  $\xi_{t+1}$ .

Predicting the next query is autoregressive, which makes language models suitable policies. Model architectures range from LSTMs [Hochreiter and Schmidhuber, 1997] to transformers such as BERT [Devlin et al., 2019] and decoder-only LLMs (e.g., GPT-4, LLaMA 3). As neural networks, these models can be designed to handle inputs and outputs in either continuous or discrete spaces, making them applicable to various domains. This allows them to support both continuous and discrete  $\mathcal{X}$  and  $\mathcal{A}$ . In discrete domains such as drug design, where molecules are represented as strings, LookaHES embeds tokens into continuous space (analogous to sentence embeddings in NLP). Differentiation through discrete outputs is handled using the reparameterization trick [Kingma and Welling, 2014] for small action sets, or policy-gradient methods such as REINFORCE [Williams, 1992], which employ the log-derivative trick, for larger and more complex ones [Mohamed et al., 2020].

### 3.5 Pathwise Sampling for Trajectory Rollout

We use pathwise sampling for the posterior predictive distribution to reduce the number of trajectories from exponential to constant. Specifically, we factorize  $p(y_{1:T} | x_{1:T}, D_0) = \int p(f | D_0) \prod_{t=1}^T p(y_t | x_t, f) df$ . At each step  $t$ , we draw a sample  $f_t \sim p(f | D_t)$  and then generate  $y_t = f_t(x_t)$ . To approximate the posterior predictive, we begin with a fixed number of restarts  $r$ , so the number of trajectories equals the number of restarts rather than growing exponentially with  $T$  (see Figure 7). We discuss the complexity trade-offs in Appendix C. Objective (2) can be formulated as

$$\xi^* = \arg \inf_{\xi \in \Xi} \frac{1}{r} \sum_{\tau=1}^r \left[ \inf_{a \in \mathcal{A}} [\ell(f_t^{(\tau)}, a) + \lambda c(x_{1:t}, x_{1:L}, a)] \right],$$

where  $f_t^{(\tau)} \sim p(f | D_t)$ , and  $y_{1:L}^{(\tau)} = f_t^{(\tau)}(x_{1:L})$ .

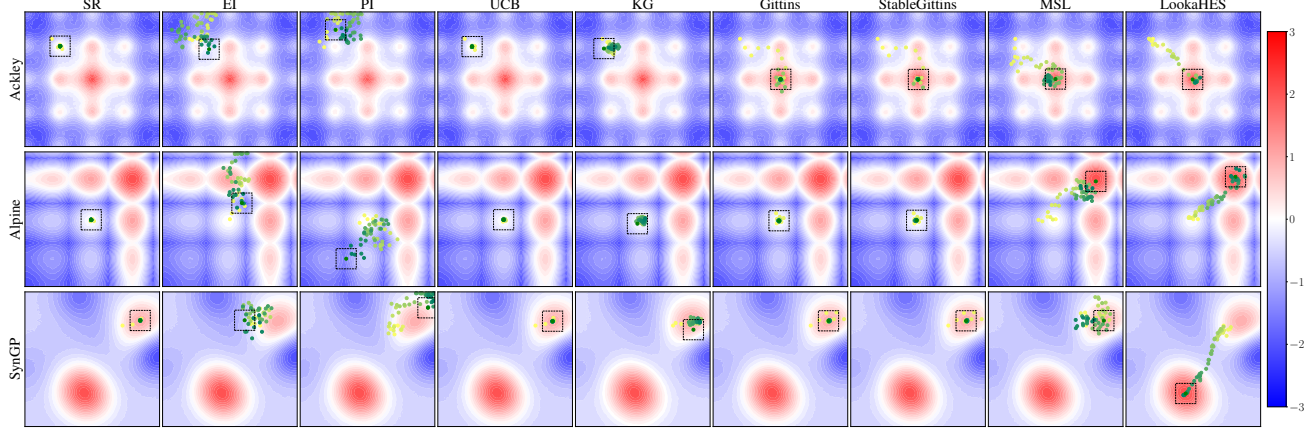


Figure 3: Queries across BO iterations with  $\sigma = 0.05$  and  $r$ -spotlight cost. Yellow and green points indicate the initial position and final action, respectively. LookaHES reaches the global optimum, whereas the others tend to be trapped in local optima.

## 4 Experiments and Results

In the following section, we compare the performance and robustness of LookaHES through a series of experiments designed to address three objectives. First, we demonstrate the algorithm’s ability to efficiently optimize in environments with dynamically varying query costs. Second, we benchmark its performance against established baselines across both synthetic and real-world scenarios. Third, we highlight its practical advantages in terms of solution quality and computational efficiency. Collectively, these experiments aim to answer the following research questions.

- **RQ1:** How does the proposed method compare to state-of-the-art myopic and nonmyopic acquisition functions in the continuous input domain under dynamic cost constraints?
- **RQ2:** Is it possible to apply the proposed method to problems with discrete input spaces?
- **RQ3:** How do aleatoric and epistemic noises, the quality of the surrogate model, and the lookahead horizon impact the performance of LookaHES?
- **RQ4:** Does ‘optimism’ in myopic methods lead to better performance than nonmyopic methods without optimism? Can this optimism be broadly applied to real-world problems?

We compare LookaHES with eight baselines implemented with BoTorch [Balandat et al., 2020] including Simple Regret (SR) [Zhao et al., 2023], Expected Improvement (EI) [Mockus, 1989], Probability of Improvement (PI) [Kushner, 1964], Upper Confidence Bound (UCB) [Srinivas et al., 2010], Knowledge Gradient (KG) [Frazier et al., 2009], Gittins,

StableGittins [Xie et al., 2024], and Multistep Tree (MSL) [Jiang et al., 2020b]. Details of these baselines are presented in Appendix D. All acquisition function values are estimated via the quasi-Monte Carlo method with the Sobol sequence [Balandat et al., 2020]. We experiment with four cost functions, including Euclidean, Manhattan,  $r$ -spotlight, and non-Markovian cost based on Euclidean distance. We use the Sample Average Approximation with a base sample as a variance reduction technique, which significantly improves the stability of the optimization. All optimizations are conducted with 64 restarts, employing the default value of  $\lambda = 1$  to regulate the DM’s budget allocation. The lookahead horizon is set to 20 for both LookaHES and Multistep Tree. Each experiment is repeated with three random seeds. All experiments are performed on an NVIDIA A100 GPU 80GB.

### 4.1 Continuous Synthetic Functions

To answer **RQ1**, we evaluate LookaHES on nine synthetic functions for global optimization in continuous spaces. The 2-dimensional functions, with their initial data points and maximum BO steps, include Ackley (50 samples, 100 steps), Alpine (100 samples, 50 steps), HolderTable (100 samples, 50 steps), Levy (100 samples, 50 steps), Styblinski-Tang (50 samples, 50 steps), and SynGP (25 samples, 50 steps). The SynGP function is sampled from a 2D RBF Gaussian Process with length scale  $\sqrt{0.25}$  and signal variance 1. High-dimensional functions include Ackley4D (4D, 100 samples, 100 steps), Hartmann (6D, 500 samples, 100 steps), and Cosine8 (8D, 200 samples, 100 steps). More details of these functions are available in [Bingham, 2013]. The variation in the number of initial samples and optimization steps reflects the complexity of each function. To evaluate the robustness of our method, we conduct

ablation studies on noise levels, initial data points, surrogate model kernels, lookahead horizon, and hyperparameter choices in the myopic acquisition function, as detailed in Appendix E.

**Summary:** LookaHES consistently outperforms the myopic and is comparable to nonmyopic baselines on synthetic functions, highlighting the advantage of a long lookahead horizon.

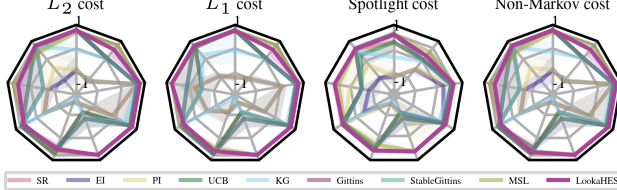


Figure 4: Final observed value at  $\sigma = 0.05$ . From the north of each plot, counter-clockwise: Ackley, Ackley4D, Alpine, Cosine8, Hartmann, HolderTable, Levy, StyblinskiTang, SynGP. LookaHES consistently found global optimum across various cost structures.

All function inputs are normalized to the hypercube  $[0, 1]^d$ , and outputs are scaled to the range  $[-3, 3]$ . The global maximum of each function is 3, so the instantaneous regret of an action  $a$  is defined as  $3 - f^*(a)$ . Observations are corrupted with three noise levels: 0%, 1%, and 5%. We use a Gaussian Process with a Matern kernel as the surrogate model. The variational neural network consists of a two-layer encoder, a Gated Recurrent Unit, and a three-layer decoder with exponential linear unit activations and 64 hidden dimensions. This network is trained using Adam optimizer with  $10^{-3}$  learning rate. During inference, we add a small noise sampled from the von Mises–Fisher distribution [Fisher, 1953] to the predicted query to enhance the exploration and facilitate acquisition function optimization restart. Figure 3 illustrates that myopic algorithms often converge to local maxima due to their inability to account for long-term effects, leading to suboptimal solutions that seem beneficial in the short term. In contrast, LookaHES can consider future outcomes, enabling it to move toward the global maximum. With our improvements, the MSL method can achieve a lookahead of up to 20 steps, yielding outcomes similar to LookaHES. However, without the neural policy, MSL optimizes directly on decision variables, which limits its applicability to real-world scenarios, as demonstrated in the next section. Figure 4 compares the baseline methods and our proposed approach in terms of the final observed values under the highest noise level ( $\sigma = 0.05$ ) across four cost functions. We also evaluate LookaHES to a real-world problem in continuous space for identifying areas with the most light in NASA night-light imagery. The results of this experiment are presented in Appendix F.

## 4.2 Protein Sequence Design

We demonstrate the practical applicability of LookaHES to optimize protein sequences [Elnaggar et al., 2023]. The decision-making process involves determining whether to edit a given protein sequence at a single position. The spotlight cost function is applied in this experiment to simulate real situations where editing more than one position will incur unpredictable, large costs. This experiment addresses **RQ2** with real-world problems. Figure 5 (top) provides a visualization of the protein space. If editing is chosen, the next step is to determine the position to be edited and select the new amino acid. We conduct a sequence of  $T = 12$  edits to maximize the fluorescence level obtained from a wet lab experiment, given by the black-box oracle  $f^* : \mathcal{X} \rightarrow \mathbb{R}$ , which is expensive to query. We assume that  $f^*$  has a parametric functional form on the feature space  $\phi(x)$ :  $y = f_{\theta^*}(x) = g(x) + \alpha(\phi(x)^\top \theta^* + \epsilon)$ , where  $\theta^* \sim p(\theta) = \mathcal{N}(\mu, \Sigma)$ ,  $\epsilon \sim \mathcal{N}(0, \sigma)$ ,  $g(\cdot)$  is a synthetic function, and  $\alpha$  is a scaling hyperparameter.

We utilize the ProteinEA Fluorescence dataset [ProteinEA, 2024], which comprises 21,445 training samples, to construct the black-box oracle. We experiment with various feature extraction functions  $\phi(\cdot)$ , including LLaMa-2 7B [Touvron et al., 2023], LLaMa-3 8B [Meta, 2024], Mistral 7B [Jiang et al., 2023], Gemma 7B [GemmaTeam, 2024], ESM-2 650M, ESM-2 3B [Lin et al., 2022], and Llama-Molst-Protein 7B [Fang et al., 2024]. Figure 17 shows validation results of the parametric black-box oracle with varying training sample sizes. Gemma 7B achieves the highest validation  $R^2$  for predicting fluorescence, so we use it as the feature extraction for all methods.

Next, we construct our semi-synthetic protein space using a sequence from the ProteinEA Fluorescence. Specifically, we select a single sequence from the validation set consisting of 237 amino acids across 20 types. In this experiment, the protein designer can edit only one amino acid at a time across a maximum of 12 fixed positions and is limited to 2 possible amino acid types for each position. Under this setting, the protein space  $\mathcal{X}$  contains  $|\mathcal{X}| = 4096$  possible proteins. We then compute the fluorescence values for these proteins using the previously constructed oracle. The goal is to edit a starting protein to achieve the highest fluores-

cence, defined as  $x_{max} = \arg \max_{x_i \in \mathcal{X}} \mathbb{E}_{\theta^* \sim p(\theta)} f_{\theta^*}(x_i)$ . The starting protein,  $x_0$ , is chosen as the one with an edit distance of 12 from the protein with maximal fluorescence. Because each edit position can only accommodate two different tokens in this setup, there is only one possible starting protein. We choose  $\alpha = 0.2$  and  $g(x) = -0.005(d - 0.5)(d - 5)(d - 8)(d - 13.4)$ , where  $d = d_{edit}(x, x_0)$  represents the edit distance between the starting protein and a given protein  $x$ . We ablate this experiment with a different starting protein and synthetic function  $g(x)$ . The ablation results are presented in Appendix H.

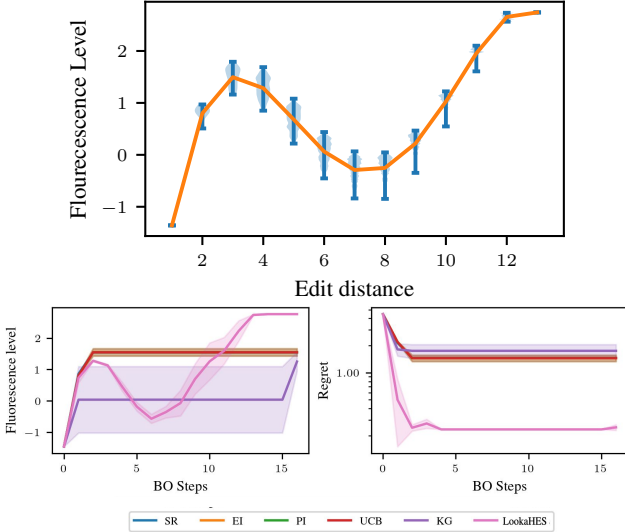


Figure 5: Fluorescence distribution by edit distance (top), observed fluorescence across BO steps (bottom left), and regret across BO steps (bottom right). Myopic methods are trapped in local minima ( $\approx 1.5$  fluorescence), while our 12-step LookaHES anticipates the global maximum, achieving  $\approx 2.7$  fluorescence.

We use a Bayesian linear regression model as a surrogate to guide optimization. At each step  $t \in [T]$ , hyperparameters are estimated via maximum marginal log-likelihood, and the next mutation is selected by optimizing the language model (Section 3). This process maximizes fluorescence, maintaining the cost constraints. The mutation and fluorescence value are given by  $x_{t+1} \sim p_{\xi_t}(x_t)$  and  $f_{\theta^*}(x_{t+1})$ , respectively, updating the dataset before the next iteration. This optimization can be batched, and we use Llama-3.2 3B as the variational network. We set the online and lookahead steps to 16 and 12, respectively. The experiments are repeated with three seeds. Before starting the optimization process, the model is supervised finetuned with random mutation data. In online iteration, we optimize the network with a maximum of 768 gradient steps and perform 64 restarts to select the next mutation. To enhance optimization efficiency, we modified Proximal

Policy Optimization (PPO) by decoupling training and inference, with vLLM [Kwon et al., 2023] handling the lookahead rollout. After each gradient update, network weights are transferred to vLLM for the next rollout. To accommodate the spotlight cost during the generation of each lookahead sequence, we employ an iterative approach, attempting to regenerate the sequence up to 32 times. If regeneration is unsuccessful, we randomly mutate to the most recent sequence, with a 50% probability of retaining it unmodified. Figure 5 (bottom left) shows the observed fluorescence levels, while the (bottom right) side presents the regret ( $3 - f_{\theta^*}(a)$ ) across online iterations. More details about our experiments can be found in Appendix G.

Under the single-edit constraint, myopic acquisitions stall in a local basin ( $\approx 1.5$  fluorescence), whereas our 12-step LookaHES leverages bridge edits to reach the  $\approx 2.7$  mode with lower cumulative regret. Mechanistically, lookahead enlarges the decision receptive field, leading the policy to prioritize downstream access over one-step gains. As shown in Figure 5, LookaHES advances across edit-distance steps before descending into the global basin, whereas myopic methods oscillate locally and repeatedly sample low-yield variants, missing the nonlocal route to the optimum.

**Summary:** LookaHES works well on discrete domains, including the protein editing task, with superior performance to other myopic approaches, proving its effectiveness across diverse applications.

## 5 Discussion, Limitations, and Future Work

We propose LookaHES for the nonmyopic BO in dynamic cost settings. LookaHES incorporates dynamic costs and downstream utility, leading to more informed decision-making under uncertainty. By utilizing a neural network policy, it achieves scalability in planning multiple steps ahead. Experimental results demonstrate its outstanding performance compared to baseline methods on various benchmarks. However, the method has limitations. It requires a well-defined cost model upfront, which may not always be practical, and its performance relies heavily on a well-specified surrogate model. Future work should explore the impact of model misspecification on plan quality. Further advancements in adaptive modeling and cost estimation could enhance its robustness, expanding its applicability to even more complex decision-making scenarios.

## References

[Aglietti et al., 2021] Aglietti, V., Dhir, N., González, J., and Damoulas, T. (2021). Dynamic causal Bayesian optimization. In *Advances in Neural Information Processing Systems*, volume 35.

[Amos, 2023] Amos, B. (2023). Tutorial on amortized optimization. *Found. Trends Mach. Learn.*, 16(5):592–732.

[Astudillo et al., 2021] Astudillo, R., Jiang, D., Balandat, M., Bakshy, E., and Frazier, P. (2021). Multi-step budgeted Bayesian optimization with unknown evaluation costs. *Advances in Neural Information Processing Systems*, 34:20197–20209.

[Balandat et al., 2020] Balandat, M., Karrer, B., Jiang, D. R., Daulton, S., Letham, B., Wilson, A. G., and Bakshy, E. (2020). BoTorch: A Framework for Efficient Monte-Carlo Bayesian Optimization. In *Advances in Neural Information Processing Systems* 33.

[Belakaria et al., 2023] Belakaria, S., Doppa, J. R., Fusi, N., and Sheth, R. (2023). Bayesian optimization over iterative learners with structured responses: A budget-aware planning approach. In *International Conference on Artificial Intelligence and Statistics*, pages 9076–9093. Proceedings of Machine Learning Research.

[Belanger et al., 2019] Belanger, D., Vora, S., Mariet, Z., Deshpande, R., Dohan, D., Angermueller, C., Murphy, K., Chapelle, O., and Colwell, L. (2019). Biological sequence design using batched Bayesian optimization. In *NeurIPS 2019 Workshop on Machine Learning and the Physical Sciences*.

[Bengio et al., 2013] Bengio, Y., Léonard, N., and Courville, A. C. (2013). Estimating or propagating gradients through stochastic neurons for conditional computation. *ArXiv*, abs/1308.3432.

[Bingham, 2013] Bingham, D. (2013). Optimization test problems. <https://www.sfu.ca/~ssurjano/optimization.html>. Accessed: 2024-09-01.

[Błażej et al., 2017] Błażej, P., Mackiewicz, D., Grabińska, M., Wnętrzak, M., and Mackiewicz, P. (2017). Optimization of amino acid replacement costs by mutational pressure in bacterial genomes. *Scientific Reports*, 7(1):1061.

[Bordas et al., 2020] Bordas, R., Heritage, J., Javed, M., Peacock, G., Taha, T., Ward, P., Vernon, I., and Hammersley, R. (2020). A Bayesian optimisation workflow for field development planning under geological uncertainty. *European Association of Geoscientists and Engineers*, 2020(1):1–20.

[Caraus et al., 2015] Caraus, I., Alsuwailem, A. A., Nadon, R., and Makarenkov, V. (2015). Detecting and overcoming systematic bias in high-throughput screening technologies: a comprehensive review of practical issues and methodological solutions. *Briefings in Bioinformatics*, 16(6):974–986.

[Carta et al., 2023] Carta, T., Romac, C., Wolf, T., Lamprier, S., Sigaud, O., and Oudeyer, P.-Y. (2023). Grounding large language models in interactive environments with online reinforcement learning. In *Proceedings of the 40th International Conference on Machine Learning*, ICML’23. JMLR.org.

[Cheon et al., 2025] Cheon, M., Lee, J. H., Koh, D.-Y., and Tsay, C. (2025). EARL-BO: Reinforcement learning for multi-step lookahead, high-dimensional bayesian optimization. In *Forty-second International Conference on Machine Learning*.

[DeGroot, 1962] DeGroot, M. H. (1962). Uncertainty, information, and sequential experiments. *The Annals of Mathematical Statistics*, 33(2):404–419.

[Devlin et al., 2019] Devlin, J., Chang, M.-W., Lee, K., and Toutanova, K. (2019). BERT: Pre-training of deep bidirectional transformers for language understanding. In Burstein, J., Doran, C., and Solorio, T., editors, *Proceedings of the 2019 Conference of the North American Chapter of the Association for Computational Linguistics: Human Language Technologies, Volume 1 (Long and Short Papers)*, pages 4171–4186, Minneapolis, Minnesota. Association for Computational Linguistics.

[Elnaggar et al., 2023] Elnaggar, A., Essam, H., Salah-Eldin, W., Moustafa, W., Elkerdawy, M., Rochereau, C., and Rost, B. (2023). Ankh: Optimized protein language model unlocks general-purpose modelling.

[Ez-zizi et al., 2023] Ez-zizi, A., Farrell, S., Leslie, D., Malhotra, G., and Ludwig, C. J. H. (2023). Reinforcement learning under uncertainty: Expected versus unexpected uncertainty and state versus reward uncertainty. *Computational Brain & Behavior*, 6(4):626–650.

[Fang et al., 2024] Fang, Y., Liang, X., Zhang, N., Liu, K., Huang, R., Chen, Z., Fan, X., and Chen, H. (2024). Mol-instructions: A large-scale biomolecular instruction dataset for large language models. In *The Twelfth International Conference on Learning Representations*.

[Fisher, 1953] Fisher, R. A. (1953). Dispersion on a sphere. *Proceedings of the Royal Society of London. Series A. Mathematical and Physical Sciences*, 217(1130):295–305.

[Folch et al., 2024] Folch, J. P., Tsay, C., Lee, R. M., Shafei, B., Ormaniec, W., Krause, A., van der Wilk, M., Misener, R., and Mutny, M. (2024). Transition constrained bayesian optimization via markov decision processes. In *The Thirty-eighth Annual Conference on Neural Information Processing Systems*.

[Folch et al., 2022] Folch, J. P., Zhang, S., Lee, R. M., Shafei, B., Walz, D., Tsay, C., van der Wilk, M., and Misener, R. (2022). SnAKE: Bayesian optimization with pathwise exploration. In Oh, A. H., Agarwal, A., Belgrave, D., and Cho, K., editors, *Advances in Neural Information Processing Systems*.

[Foster et al., 2021] Foster, A., Ivanova, D. R., Malik, I., and Rainforth, T. (2021). Deep adaptive design: Amortizing sequential Bayesian experimental design. In *International Conference on Machine Learning*.

[Foster et al., 2019] Foster, A., Jankowiak, M., Bingham, E., Horsfall, P., Teh, Y. W., Rainforth, T., and Goodman, N. (2019). Variational bayesian optimal experimental design. In *Proceedings of the 33rd International Conference on Neural Information Processing Systems*, Red Hook, NY, USA. Curran Associates Inc.

[Frazier et al., 2009] Frazier, P., Powell, W., and Dayanik, S. (2009). The knowledge-gradient policy for correlated normal beliefs. *INFORMS journal on Computing*, 21(4):599–613.

[Frazier, 2018] Frazier, P. I. (2018). A tutorial on Bayesian optimization. *INFORMS Tutorials in Operations Research*.

[Garcia and Rachelson, 2013] Garcia, F. and Rachelson, E. (2013). *Markov decision processes*. Wiley Online Library.

[Garnett, 2022] Garnett, R. (2022). *Bayesian Optimization*. Cambridge University Press.

[GemmaTeam, 2024] GemmaTeam (2024). Gemma: Open models based on gemini research and technology.

[González et al., 2016] González, J., Osborne, M., and Lawrence, N. (2016). GLASSES: Relieving the myopia of Bayesian optimisation. In *Artificial Intelligence and Statistics*, pages 790–799. Proceedings of Machine Learning Research.

[Guo et al., 2004] Guo, H. H., Choe, J., and Loeb, L. A. (2004). Protein tolerance to random amino acid change. *Proceedings of the National Academy of Sciences*, 101(25):9205–9210.

[Hafner et al., 2021] Hafner, D., Lillicrap, T. P., Norouzi, M., and Ba, J. (2021). Mastering Atari with discrete world models. In *International Conference on Learning Representations*.

[Hamed et al., 2024] Hamed, H., Kim, S., Kim, D., Yoon, J., and Ahn, S. (2024). Dr. strategy: Model-based generalist agents with strategic dreaming. In *Forty-first International Conference on Machine Learning*.

[Harper et al., 2019] Harper, E., Majumdar, S., Kuchaiev, O., et al. (2019). NeMo: a toolkit for Conversational AI and Large Language Models. <https://nvidia.github.io/NeMo>.

[Hazra et al., 2024] Hazra, R., Dos Martires, P. Z., and De Raedt, L. (2024). SayCanPay: Heuristic planning with large language models using learnable domain knowledge. In *Proceedings of the AAAI Conference on Artificial Intelligence*, volume 38, pages 20123–20133.

[Hochreiter and Schmidhuber, 1997] Hochreiter, S. and Schmidhuber, J. (1997). Long short-term memory. *Neural computation*, 9(8):1735–1780.

[Hu et al., 2025] Hu, J., Wu, X., Shen, W., Liu, J. K., Wang, W., Jiang, S., Wang, H., Chen, H., Chen, B., Fang, W., Xianyu, Cao, Y., Xu, H., and Liu, Y. (2025). OpenRLHF: A ray-based easy-to-use, scalable and high-performance RLHF framework. In Habernal, I., Schulam, P., and Tiedemann, J., editors, *Proceedings of the 2025 Conference on Empirical Methods in Natural Language Processing: System Demonstrations*, pages 656–666, Suzhou, China. Association for Computational Linguistics.

[Hubert et al., 2021] Hubert, T., Schrittwieser, J., Antonoglou, I., Barekatain, M., Schmitt, S., and Silver, D. (2021). Learning and planning in complex action spaces. In Meila, M. and Zhang, T., editors, *Proceedings of the 38th International Conference on Machine Learning*, volume 139 of *Proceedings of Machine Learning Research*, pages 4476–4486. PMLR.

[Ivanova et al., 2021] Ivanova, D. R., Foster, A., Klein gesse, S., Gutmann, M. U., and Rainforth, T. (2021). Implicit deep adaptive design: policy-based experimental design without likelihoods. *Advances in Neural Information Processing Systems*, 34:25785–25798.

[Janner et al., 2019] Janner, M., Fu, J., Zhang, M., and Levine, S. (2019). When to trust your model: model-based policy optimization. In *Proceedings of the 33rd International Conference on Neural Information Processing Systems*, Red Hook, NY, USA. Curran Associates Inc.

[Jiang et al., 2023] Jiang, A. Q., Sablayrolles, A., Mensch, A., Bamford, C., Chaplot, D. S., de las Casas, D., Bressand, F., Lengyel, G., Lample, G., Saulnier, L., Lavaud, L. R., Lachaux, M.-A., Stock, P., Scao, T. L., Lavril, T., Wang, T., Lacroix, T., and Sayed, W. E. (2023). Mistral 7b. 611–626, New York, NY, USA. Association for Computing Machinery.

[Jiang et al., 2020a] Jiang, S., Chai, H., Gonzalez, J., and Garnett, R. (2020a). BINOCULARS for efficient, nonmyopic sequential experimental design. In *International Conference on Machine Learning*, pages 4794–4803. Proceedings of Machine Learning Research.

[Jiang et al., 2020b] Jiang, S., Jiang, D., Balandat, M., Karrer, B., Gardner, J., and Garnett, R. (2020b). Efficient nonmyopic Bayesian optimization via one-shot multi-step trees. *Advances in Neural Information Processing Systems*, 33:18039–18049.

[Kandasamy et al., 2018] Kandasamy, K., Krishnamurthy, A., Schneider, J., and Poczos, B. (2018). Parallelised Bayesian optimisation via Thompson sampling. In Storkey, A. and Perez-Cruz, F., editors, *Proceedings of the Twenty-First International Conference on Artificial Intelligence and Statistics*, volume 84 of *Proceedings of Machine Learning Research*, pages 133–142. PMLR.

[Kharkovskii et al., 2020] Kharkovskii, D., Ling, C. K., and Low, B. K. H. (2020). Nonmyopic gaussian process optimization with macro-actions. In Chiappa, S. and Calandra, R., editors, *Proceedings of the Twenty Third International Conference on Artificial Intelligence and Statistics*, volume 108 of *Proceedings of Machine Learning Research*, pages 4593–4604. PMLR.

[Kingma and Welling, 2014] Kingma, D. P. and Welling, M. (2014). Auto-encoding variational bayes. *ICLR*.

[Kushner, 1964] Kushner, H. (1964). A new method of locating the maximum point of an arbitrary multi-peak curve in the presence of noise. *Journal of Basic Engineering*, 86(1):97–106.

[Kushner, 1962] Kushner, H. J. (1962). A versatile stochastic model of a function of unknown and time varying form. *Journal of Mathematical Analysis and Applications*, 5(1):150–167.

[Kwon et al., 2023] Kwon, W., Li, Z., Zhuang, S., Sheng, Y., Zheng, L., Yu, C. H., Gonzalez, J., Zhang, H., and Stoica, I. (2023). Efficient memory management for large language model serving with page-dattention. In *Proceedings of the 29th Symposium on Operating Systems Principles*, SOSP ’23, page 611–626, New York, NY, USA. Association for Computing Machinery.

[Lam et al., 2016] Lam, R., Willcox, K., and Wolpert, D. H. (2016). Bayesian optimization with a finite budget: An approximate dynamic programming approach. *Advances in Neural Information Processing Systems*, 29.

[Lee et al., 2020] Lee, E., Eriksson, D., Bindel, D., Cheng, B., and McCourt, M. (2020). Efficient rollout strategies for Bayesian optimization. In *Conference on Uncertainty in Artificial Intelligence*, pages 260–269. Proceedings of Machine Learning Research.

[Lee et al., 2021] Lee, E. H., Eriksson, D., Perrone, V., and Seeger, M. (2021). A nonmyopic approach to cost-constrained Bayesian optimization. In de Campos, C. and Maathuis, M. H., editors, *Proceedings of the Thirty-Seventh Conference on Uncertainty in Artificial Intelligence*, volume 161 of *Proceedings of Machine Learning Research*, pages 568–577. PMLR.

[Lin et al., 2022] Lin, Z., Akin, H., Rao, R., Hie, B., Zhu, Z., Lu, W., Smetanin, N., dos Santos Costa, A., Fazel-Zarandi, M., Sercu, T., Candido, S., et al. (2022). Language models of protein sequences at the scale of evolution enable accurate structure prediction. *bioRxiv*.

[Ling et al., 2016] Ling, C. K., Low, K. H., and Jaillet, P. (2016). Gaussian Process Planning with Lipschitz Continuous Reward Functions: Towards Unifying Bayesian Optimization, Active Learning, and Beyond. *Proceedings of the AAAI Conference on Artificial Intelligence*, 30(1).

[Liu et al., 2023] Liu, P., Wang, H., and Qiyu, W. (2023). Bayesian optimization with switching cost: Regret analysis and lookahead variants. In Elkind, E., editor, *Proceedings of the Thirty-Second International Joint Conference on Artificial Intelligence, IJCAI-23*, pages 4011–4018. International Joint Conferences on Artificial Intelligence Organization. Main Track.

[Lötjens et al., 2019] Lötjens, B., Everett, M., and How, J. P. (2019). Safe reinforcement learning with model uncertainty estimates. In *2019 International Conference on Robotics and Automation (ICRA)*, page 8662–8668. IEEE Press.

[Luis et al., 2023] Luis, C. E., Bottero, A. G., Vinogradsk, J., Berkenkamp, F., and Peters, J. (2023). Model-based uncertainty in value functions. In Ruiz, F., Dy, J., and van de Meent, J.-W., editors, *Proceedings of The 26th International Conference on Artificial Intelligence and Statistics*, volume 206 of

[Proceedings of Machine Learning Research, pages 8029–8052. PMLR.

[Luong et al., 2021] Luong, P., Nguyen, D., Gupta, S., Rana, S., and Venkatesh, S. (2021). Adaptive cost-aware bayesian optimization. *Knowledge-Based Systems*, 232:107481.

[Maraval et al., 2023] Maraval, A. M., Zimmer, M., Grosnit, A., and Ammar, H. B. (2023). End-to-end meta-bayesian optimisation with transformer neural processes. In *Thirty-seventh Conference on Neural Information Processing Systems*.

[Meta, 2024] Meta (2024). Llama 3 model card.

[Minderer et al., 2021] Minderer, M., Djolonga, J., Romijnders, R., Hubis, F. A., Zhai, X., Houlsby, N., Tran, D., and Lucic, M. (2021). Revisiting the calibration of modern neural networks. In Beygelzimer, A., Dauphin, Y., Liang, P., and Vaughan, J. W., editors, *Advances in Neural Information Processing Systems*.

[Mockus, 1989] Mockus, J. (1989). Bayesian approach to global optimization: Theory and applications. In *Bayesian Approach to Global Optimization*.

[Mohamed et al., 2020] Mohamed, S., Rosca, M., Figurnov, M., and Mnih, A. (2020). Monte Carlo gradient estimation in machine learning. *Journal of Machine Learning Research*, 21(132):1–62.

[Moritz et al., 2018] Moritz, P., Nishihara, R., Wang, S., Tumanov, A., Liaw, R., Liang, E., Elibol, M., Yang, Z., Paul, W., Jordan, M. I., and Stoica, I. (2018). Ray: a distributed framework for emerging AI applications. In *Proceedings of the 13th USENIX Conference on Operating Systems Design and Implementation*, OSDI’18, page 561–577, USA. USENIX Association.

[Neiswanger et al., 2022] Neiswanger, W., Yu, L., Zhao, S., Meng, C., and Ermon, S. (2022). Generalizing Bayesian optimization with decision-theoretic entropies. In Oh, A. H., Agarwal, A., Belgrave, D., and Cho, K., editors, *Advances in Neural Information Processing Systems*.

[Nguyen-Tang and Arora, 2024] Nguyen-Tang, T. and Arora, R. (2024). On the statistical complexity of offline decision-making. In Salakhutdinov, R., Kolter, Z., Heller, K., Weller, A., Oliver, N., Scarlett, J., and Berkenkamp, F., editors, *Proceedings of the 41st International Conference on Machine Learning*, volume 235 of *Proceedings of Machine Learning Research*, pages 37900–37928. PMLR.

[Nwankwo and Bindel, 2024] Nwankwo, D. and Bindel, D. (2024). Differentiating policies for non-myopic bayesian optimization.

[Nyikosa et al., 2018] Nyikosa, F. M., Osborne, M. A., and Roberts, S. J. (2018). Bayesian optimization for dynamic problems.

[Osborne, 2010] Osborne, M. A. (2010). *Bayesian Gaussian processes for sequential prediction, optimization and quadrature*. PhD thesis, Oxford University, UK.

[Ouyang et al., 2024] Ouyang, L., Wu, J., Jiang, X., Almeida, D., Wainwright, C. L., Mishkin, P., Zhang, C., Agarwal, S., Slama, K., Ray, A., Schulman, J., Hilton, J., Kelton, F., Miller, L., Simens, M., Askell, A., Welinder, P., Christiano, P., Leike, J., and Lowe, R. (2024). Training language models to follow instructions with human feedback. In *Proceedings of the 36th International Conference on Neural Information Processing Systems*, NeurIPS ’22, Red Hook, NY, USA. Curran Associates Inc.

[Palo et al., 2023] Palo, N. D., Byravan, A., Hasen- clever, L., Wulfmeier, M., Heess, N., and Riedmiller, M. (2023). Towards a unified agent with foundation models. In *Workshop on Reincarnating Reinforcement Learning at ICLR 2023*.

[ProteinEA, 2024] ProteinEA (2024). Fluorescence Dataset. <https://huggingface.co/datasets/proteinea/fluorescence>. Accessed: 2024-05-02.

[Puterman, 2014] Puterman, M. L. (2014). *Markov decision processes: discrete stochastic dynamic programming*. John Wiley & Sons.

[Quiñonero-Candela and Rasmussen, 2005] Quiñonero-Candela, J. and Rasmussen, C. E. (2005). A unifying view of sparse approximate Gaussian process regression. *Journal of Machine Learning Research*, 6(65):1939–1959.

[Russo and Van Roy, 2016] Russo, D. and Van Roy, B. (2016). An information-theoretic analysis of Thompson sampling. *Journal of Machine Learning Research*, 17(68):1–30.

[Schrödinger, LLC, 2015] Schrödinger, LLC (2015). The PyMOL molecular graphics system, version 1.8. <https://pymol.org/2/>. Accessed: 2024-12-16.

[Schulman et al., 2017] Schulman, J., Wolski, F., Dhariwal, P., Radford, A., and Klimov, O. (2017). Proximal policy optimization algorithms.

[Shahriari et al., 2016] Shahriari, B., Swersky, K., Wang, Z., Adams, R. P., and de Freitas, N. (2016).

Taking the human out of the loop: A review of Bayesian optimization. *Proceedings of the IEEE*, 104(1):148–175.

[Snoek et al., 2012] Snoek, J., Larochelle, H., and Adams, R. P. (2012). Practical bayesian optimization of machine learning algorithms. In Pereira, F., Burges, C., Bottou, L., and Weinberger, K., editors, *Advances in Neural Information Processing Systems*, volume 25. Curran Associates, Inc.

[Srinivas et al., 2010] Srinivas, N., Krause, A., Kakade, S., and Seeger, M. (2010). Gaussian process optimization in the bandit setting: no regret and experimental design. In *Proceedings of the 27th International Conference on International Conference on Machine Learning*, pages 1015–1022.

[Stolze et al., 2015] Stolze, B., Reinhart, S., Bullinger, L., Fröhling, S., and Scholl, C. (2015). Comparative analysis of kras codon 12, 13, 18, 61 and 117 mutations using human mcf10a isogenic cell lines. *Scientific Reports*, 5(1):8535.

[Sun et al., 2024] Sun, J., Jiang, Y., Qiu, J., Nobel, P. T., Kochenderfer, M., and Schwager, M. (2024). Conformal prediction for uncertainty-aware planning with diffusion dynamics model. In *Proceedings of the 37th International Conference on Neural Information Processing Systems*, NeurIPS ’23, Red Hook, NY, USA. Curran Associates Inc.

[Thompson, 1933] Thompson, W. R. (1933). On the likelihood that one unknown probability exceeds another in view of the evidence of two samples. *Biometrika*, 25:285–294.

[Touvron et al., 2023] Touvron, H. et al. (2023). Llama 2: Open foundation and fine-tuned chat models.

[Treven et al., 2024] Treven, L., Hübotter, J., Sukhija, B., Krause, A., and Dörfler, F. (2024). Efficient exploration in continuous-time model-based reinforcement learning. In *Proceedings of the 37th International Conference on Neural Information Processing Systems*, NeurIPS ’23, Red Hook, NY, USA. Curran Associates Inc.

[von Werra et al., 2020] von Werra, L., Belkada, Y., Tunstall, L., Beeching, E., Thrush, T., Lambert, N., Huang, S., Rasul, K., and Gallouédec, Q. (2020). TRL: Transformer Reinforcement Learning. <https://github.com/huggingface/trl>.

[Šaltenis, 1971] Šaltenis, V. R. (1971). One method of multiextremum optimization. *Avtomatika i Vychislitel'naya Tekhnika (Automatic Control and Computer Sciences)*, 5(3):33–38.

[Wang and Ba, 2020] Wang, T. and Ba, J. (2020). Exploring model-based planning with policy networks. In *International Conference on Learning Representations*.

[Williams, 1992] Williams, R. J. (1992). Simple statistical gradient-following algorithms for connectionist reinforcement learning. *Machine Learning*, 8(3):229–256.

[Wilson et al., 2020] Wilson, J. T., Borovitskiy, V., Terenin, A., Mostowsky, P., and Deisenroth, M. P. (2020). Efficiently sampling functions from Gaussian process posteriors. In *Proceedings of the 37th International Conference on Machine Learning*, ICML’20. JMLR.org.

[Wu and Frazier, 2019] Wu, J. and Frazier, P. (2019). Practical two-step lookahead Bayesian optimization. *Advances in neural information processing systems*, 32.

[Xie et al., 2024] Xie, Q., Astudillo, R., Frazier, P. I., Scully, Z., and Terenin, A. (2024). Cost-aware bayesian optimization via the pandora’s box gittins index. In *Proceedings of the 38th International Conference on Neural Information Processing Systems*, NIPS ’24, Red Hook, NY, USA. Curran Associates Inc.

[Yue and Kontar, 2020] Yue, X. and Kontar, R. A. (2020). Why non-myopic Bayesian optimization is promising, and how far should we look ahead? a study via rollout. In *International Conference on Artificial Intelligence and Statistics*, pages 2808–2818. Proceedings of Machine Learning Research.

[Zangirolami and Borrotti, 2024] Zangirolami, V. and Borrotti, M. (2024). Dealing with uncertainty: Balancing exploration and exploitation in deep recurrent reinforcement learning. *Knowledge-Based Systems*, 293:111663.

[Zhang et al., 2024] Zhang, B., Mao, H., Ruan, J., Wen, Y., Li, Y., Zhang, S., Xu, Z., Li, D., Li, Z., Zhao, R., Li, L., and Fan, G. (2024). Controlling large language model-based agents for large-scale decision-making: An actor-critic approach.

[Zhao et al., 2024] Zhao, S., Kim, M. P., Sahoo, R., Ma, T., and Ermon, S. (2024). Calibrating predictions to decisions: a novel approach to multi-class calibration. In *Proceedings of the 35th International Conference on Neural Information Processing Systems*, NeurIPS ’21, Red Hook, NY, USA. Curran Associates Inc.

[Zhao et al., 2023] Zhao, Y., Stephens, C. J., Szepesvári, C., and Jun, K.-S. (2023). Revisiting

simple regret: fast rates for returning a good arm. In *Proceedings of the 40th International Conference on Machine Learning*, ICML'23. JMLR.org.

[Zheng et al., 2024] Zheng, Y., Zhang, R., Zhang, J., Ye, Y., and Luo, Z. (2024). LlamaFactory: Unified efficient fine-tuning of 100+ language models. In Cao, Y., Feng, Y., and Xiong, D., editors, *Proceedings of the 62nd Annual Meeting of the Association for Computational Linguistics (Volume 3: System Demonstrations)*, pages 400–410, Bangkok, Thailand. Association for Computational Linguistics.

[Zhou et al., 2024] Zhou, Y., Zanette, A., Pan, J., Levine, S., and Kumar, A. (2024). ArCHer: Training language model agents via hierarchical multi-turn RL. In *Proceedings of the 41st International Conference on Machine Learning*, ICML'24. JMLR.org.

[Zhu et al., 2025] Zhu, W. B., Singh, I., Jia, R., and Thomason, J. (2025). Language models can infer action semantics for symbolic planners from environment feedback. In Chiruzzo, L., Ritter, A., and Wang, L., editors, *Proceedings of the 2025 Conference of the Nations of the Americas Chapter of the Association for Computational Linguistics: Human Language Technologies (Volume 1: Long Papers)*, pages 8751–8773, Albuquerque, New Mexico. Association for Computational Linguistics.

[Zhuang et al., 2024] Zhuang, Y., Chen, X., Yu, T., Mitra, S., Bursztyn, V., Rossi, R. A., Sarkhel, S., and Zhang, C. (2024). Toolchain\*: Efficient action space navigation in large language models with A\* search. In *The Twelfth International Conference on Learning Representations*.

## Checklist

- For all models and algorithms presented, check if you include:
  - A clear description of the mathematical setting, assumptions, algorithm, and/or model. [Yes. Section 3]
  - An analysis of the properties and complexity (time, space, sample size) of any algorithm. [Yes. Appendix C]
  - (Optional) Anonymized source code, with specification of all dependencies, including external libraries. [Yes. Abstract]
- For any theoretical claim, check if you include:
  - Statements of the full set of assumptions of all theoretical results. [Yes. Section 3]
  - Complete proofs of all theoretical results. [Yes. Appendix C]
- Clear explanations of any assumptions. [Yes. Section 1, 3]
- For all figures and tables that present empirical results, check if you include:
  - The code, data, and instructions needed to reproduce the main experimental results (either in the supplemental material or as a URL). [Yes. Abstract]
  - All the training details (e.g., data splits, hyperparameters, how they were chosen). [Yes. Section 4, Appendix F, G]
  - A clear definition of the specific measure or statistics and error bars (e.g., with respect to the random seed after running experiments multiple times). [Yes. Section 4, Appendix E, F]
  - A description of the computing infrastructure used. (e.g., type of GPUs, internal cluster, or cloud provider). [Yes. Section 4]
- If you are using existing assets (e.g., code, data, models) or curating/releasing new assets, check if you include:
  - Citations of the creator If your work uses existing assets. [Yes. Section 4.2]
  - The license information of the assets, if applicable. [Not Applicable]
  - New assets either in the supplemental material or as a URL, if applicable. [Yes. Abstract]
  - Information about consent from data providers/curators. [Not Applicable]
  - Discussion of sensible content if applicable, e.g., personally identifiable information or offensive content. [Not Applicable]
- If you used crowdsourcing or conducted research with human subjects, check if you include:
  - The full text of instructions given to participants and screenshots. [Not Applicable]
  - Descriptions of potential participant risks, with links to Institutional Review Board (IRB) approvals if applicable. [Not Applicable]
  - The estimated hourly wage paid to participants and the total amount spent on participant compensation. [Not Applicable]

## Supplementary Materials

### A Notation

Table 2 is a glossary of the mathematical notation used in the paper.

Table 2: Glossary of Mathematical Notation

Symbol	Description
$f^*$	Black-box function
$p(f)$	Prior distribution over the black-box function
$\theta$	Random variable representing the parameters of the black-box function in the parametric form
$\theta^*$	Optimal parameters of the black-box function in the parametric form
$\mathcal{X}$	Input domain
$\mathcal{Y}$	Output domain
$\xi$	Parameters of the variational network
$D_t$	$D_t = \{(x_i, y_i)\}_{i=1}^t$ Dataset acquired
$p_t(\cdot)$	The posterior distribution conditioned on the data up to and including timestep $t$
$c(\cdot, \dots, \cdot)$	$c : \mathcal{X}^k \rightarrow \mathbb{R}$ , cost function depending on $k$ -step history of query
$[T]$	$\{1, \dots, T\}$
$\mathbb{H}_{\ell, \mathcal{A}}$	The decision-theoretic entropy [DeGroot, 1962] corresponding to a loss function $\ell$ and an action set $\mathcal{A}$
$L$	Lookahead horizon
$T$	Number of interactions with the environment

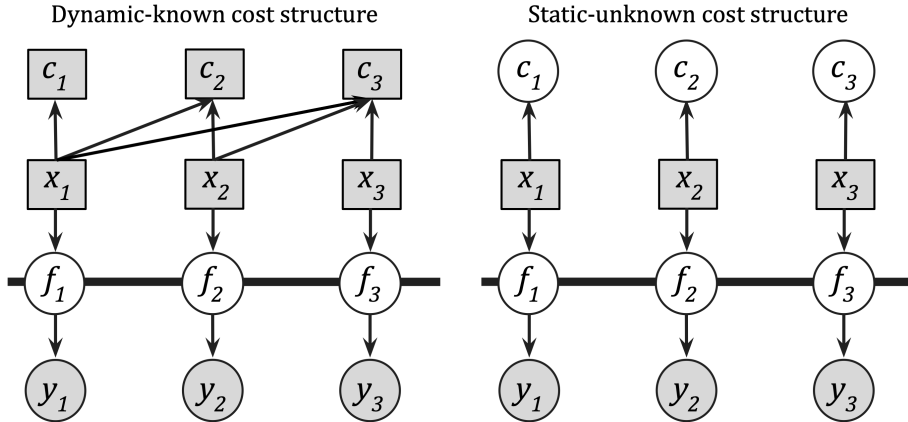


Figure 6: Graphical models of popular cost structures. In this diagram,  $f$  represents the target black-box function,  $x$  denotes the input query,  $y$  is the output value, and  $c$  is the cost of querying  $x$ . On the left — the dynamic-known cost structure — the cost of querying  $x_3$  can depend on  $x_1$  and  $x_2$ . On the right — the static-known cost structure — the cost of querying  $x_3$  is independent of other queries.

## B Related Works

**Nonmyopic Bayesian Optimization in the Dynamic Cost Setting** Nonmyopic BO has been extensively explored in prior works [Osborne, 2010, González et al., 2016, Wu and Frazier, 2019, Jiang et al., 2020a, Lee et al., 2020, Lee et al., 2021, Astudillo et al., 2021, Folch et al., 2022, Belakaria et al., 2023, Jiang et al., 2020b]. These studies focus on converting a nested, multi-step planning problem into a single, high-dimensional optimization problem that can be solved efficiently with quasi-Monte Carlo sampling and gradient-based optimization. The advantage of having a lookahead mechanism is enlarging the receptive field—the area the decision maker can see prior to making a decision (Figure 1). This approach has gained traction in cost-aware and budget-constrained BO [Astudillo et al., 2021, Lee et al., 2021], where nonmyopic planning is crucial. However, a notable challenge with this methodology is its limited scalability when extending the lookahead horizon, primarily due to the exponential increase in the number of decision variables. Our approach introduces a novel combination of Thompson sampling [Thompson, 1933] with the extensive generalization capabilities of a variational network, significantly enhancing the computational efficiency of nonmyopic BO. Utilizing neural networks for variational inference and optimization is not a new concept [Kingma and Welling, 2014, Amos, 2023]. For instance, Deep Adaptive Design [Foster et al., 2021, Ivanova et al., 2021] is a parallel line of research from the Bayesian optimal experimental design literature, which has a related but distinct objective to reduce the uncertainty of model parameters as opposed to the global optimization objective in BO. The authors concentrate on reducing the computational demands during deployment and determining the most informative experimental designs by upfront offline optimization of a neural network to amortize the design cost. Our approach diverges by aligning more closely with the principles of online Bayesian optimization. Here, the primary objective extends beyond mere information acquisition to encompass the pursuit of global optimization. Our approach, which employs adaptive decision-making through online policy optimization, could be more robust than offline methods, particularly when the approximation of the reward function changes significantly between queries. This robustness arises because the online policy is updated at each BO step while the offline methods rely on transferring knowledge from learned offline data [Nguyen-Tang and Arora, 2024]. The distinctive feature of our study is implementing a pathwise, Thompson sampling-based nonmyopic acquisition function, which significantly reduces the computational cost of the iterative posterior sampling approach in [Jiang et al., 2020b]. Additionally, we present detailed comparisons of related works on different cost structures in Appendix 2.

**Variational Policy Optimization in Complex Action Spaces** In many real-world applications, decision-makers must take actions that are complex and subject to semantic constraints. Semantic constraints refer to rules or relationships that restrict the set of valid actions based on their meanings, dependencies, or contextual appropriateness. For example, in biological sequence design, semantic constraints may ensure that the mutated sequence is valid and does not unfold the protein (i.e., protein denaturalization). Recent RL research has addressed environments with such actions, which are challenging due to two main reasons: (i) the large number of potential actions [Hubert et al., 2021, Zhang et al., 2024], and (ii) the complex semantics [Carta et al., 2023] underlying each action, making them difficult to capture. Recent studies have shown that modern LLMs can effectively model semantic actions and be fine-tuned with feedback from the environment [Zhu et al., 2025, Zhang et al., 2024, Zhuang et al., 2024, Hazra et al., 2024]. Several papers demonstrate that using LLMs as policy models in reinforcement learning leads to better outcomes [Palo et al., 2023, Zhuang et al., 2024, Hazra et al., 2024]. In the field of NLP, a chatbot such as ChatGPT can be viewed as a decision-making process where the underlying LLM must understand user questions or requests to provide appropriate responses. These actions are complex and semantically rich, as even a single word can alter the meaning of a sentence. Consequently, RL methods like proximal policy optimization [Schulman et al., 2017] have been applied to refine the abilities of language models.

**Multi-turn Training Framework for LLMs** Multi-turn conversations have been shown to be more effective for managing entire dialogues [Zhou et al., 2024]. This approach can be viewed as a nonmyopic RL method that trains LLMs to achieve better conversational outcomes. Unfortunately, current RL training frameworks for LLMs, such as TRL [von Werra et al., 2020], OpenRLHF [Hu et al., 2025], LlamaFactory [Zheng et al., 2024], and Nemo [Harper et al., 2019], primarily focus on single-turn conversations. As a result, they are not suited for multi-turn conversation training. When using these frameworks, multi-turn conversations must be divided into individual single turns, which limits the LLM’s ability to manage the overall outcome of a conversation effectively.

## C Pathwise Sampling

When the surrogate model is a Gaussian Process (GP), the Monte Carlo method is employed to evaluate the posterior predictive distribution. In prior works, this is done via iterative sampling of the following factorized distribution:  $p(y_{1:T}|x_{1:T}, D_0) = \prod_{t=1}^T p(y_t|x_t, x_{<t}, y_{<t}, D_0)$ . The posterior predictive distribution at the  $t$ -th step, denoted as  $p(y_t|x_t, x_{<t}, y_{<t}, D_0)$ , can be approximated by generating  $k$  samples of  $y_t$  from the GP model. In general, the value of  $k$  varies depending on the specific problem. At iteration  $t$ , suppose that we always sample  $k$  samples from the posterior predictive distribution. The number of  $y_t$  is  $k^t$ . This number quickly explodes exponentially with the length of the lookahead horizon (Figure 7). The GP posterior predictive sampling process involves computing the square root of the covariance matrix, which is typically done via Cholesky decomposition. The complexity of this process is proved as  $\mathcal{O}(n^3)$  for exact GP or  $\mathcal{O}(m^3)$  for approximate GP where  $n$  is the total number of samples in the training dataset and  $m < n$  is the number of inducing samples [Quiñonero-Candela and Rasmussen, 2005, Wilson et al., 2020]. This evidence shows that the complexity for sampling posterior predictive distribution at step  $t$ -th is at least  $\mathcal{O}(k^t m^3)$ . One variant of this procedure that can reduce the complexity is limiting the number of sampling samples for posterior predictive approximation at further lookahead steps. For instance, at each step  $t > 1$ , we can set  $k_{t+1} = \max(k_1/2^t, 1)$ , where  $k_1$  is the predefined number of samples at the first lookahead step. In these cases, we can observe that  $\exists \tau : \forall t > \tau, \prod_{t=1}^T k_t = K$ , where  $K$  is a constant. Subsequently, the complexity at step  $t$ -th can be reduced to  $\mathcal{O}(\prod_{t=1}^T k_t m^3) = \mathcal{O}(K m^3) = \mathcal{O}(m^3)$ .

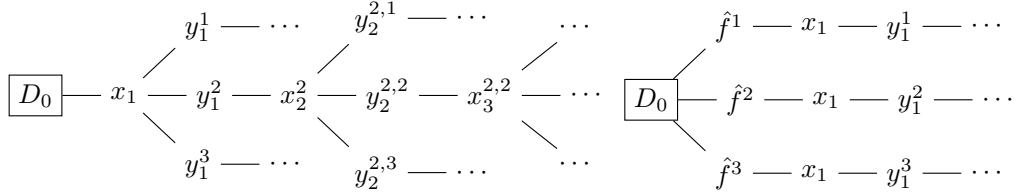


Figure 7: Posterior predictive sampling (left) and Pathwise sampling (right)

To mitigate the high complexity of above sampling process, we employ the following factorization:  $p(y_{1:T}|x_{1:T}, D_0) = \int p(y_{1:T}|x_{1:T}, f)p(f|D_0) df = \int p(f|D_0) \prod_{t=1}^T p(y_t|x_t, f) df$ . The function  $f$  is drawn from the prior distribution and path-wise updated via Matheron's rule. For the  $h$  path, consisting of  $T$  steps each, the sampling can be done with complexity  $\mathcal{O}(h \times T)$ . We can approximate the integral arbitrarily well with a higher  $h$ . The gain comes from the fact that we do not need to iteratively compute  $K_{m,m}^{-1}$  as in fantasization. If we did, the complexity, with the same number of samples, would be  $\mathcal{O}(h \times (T-1)^3)$ . This can be done in linear complexity with respect to the number of samples. The complexity of sampling a posterior  $\hat{f}$  from  $p(f|D_0)$  can be considered as  $\mathcal{O}(C)$ , where  $C$  is a constant because the number of samples in  $D_0$  is unchanged. Then, computing  $y_t$  for approximate posterior predictive  $p(y_t|x_t, \hat{f})$  can be done by  $y_t = \hat{f}(x_t)$ , which has complexity of  $\mathcal{O}(1)$ . Using the same technique as limiting the number of sampling samples, the complexity of approximating the posterior predictive at any lookahead step is  $\mathcal{O}(K)$ . Thus, the total complexity at each step  $t$ -th is  $\mathcal{O}(C + K)$ . Figure 7 (right) visualizes the concept of this method.

## D Details of Baselines

- Simple Regret (SR) [Zhao et al., 2023] measures the regret or loss in performance between the updated model and the model that would have resulted if the optimal sample had been selected for annotation during the active learning process instead.
- Expected Improvement (EI) [Mockus, 1989] is used to evaluate the usefulness of candidate samples by estimating the expected gain in the performance of a model.
- Probability of Improvement (PI) [Kushner, 1964] calculates the probability of a candidate sample improving the performance of a model compared to the current best sample.
- Upper Confidence Bound (UCB) [Srinivas et al., 2010] balances exploration and exploitation by selecting candidate samples with high uncertainty and high potential for improvement based on the upper confidence

bound of their predicted performance.

- Knowledge Gradient (KG) [Frazier et al., 2009] quantifies the expected improvement in the objective function value resulting from evaluating a specific point. It considers the uncertainty of the model predictions and the potential benefit of obtaining additional information about the objective function.
- Gittins and StableGittins [Xie et al., 2024] treat the BO problem as a Pandora’s Box problem and derive a Bayesian-optimal acquisition function by reinterpreting the Gittins index as a decision rule for selecting which point to evaluate next, given its cost and uncertainty.
- Multistep Tree (MSL) [Jiang et al., 2020b], which can look up to four steps ahead, is constrained by computational costs. We reimplement this acquisition function using Pathwise sampling, enabling a lookahead horizon of up to 20 steps.

All myopic and nonmyopic baselines are modified to include the cost function as our proposed optimization objective. Specifically, their optimization objective can be formulated as

$$x_{t+1} = \arg \inf_{x \in \mathcal{X}} (-\text{Acqf}(f, x) + \lambda c(x_{1:t}, x)).$$

## E Ablation Studies on Synthetic Functions

### E.1 Varying the Observation Noise Level

To answer the **RQ3** in terms of the impact of aleatoric noise on BO methods, we performed an ablation study by varying the observation noise levels at 0%, 1%, and 5%. A comprehensive comparison of LookaHES against baseline approaches was conducted across nine synthetic functions, incorporating all cost structures and noise levels. As shown in Figure 8, LookaHES consistently achieves superior performance across all cost structures and noise settings.

### E.2 Varying the Number of Initial Samples

In many scenarios, limited data availability at the start of an optimization process leads to a poorly constructed surrogate model, resulting in high epistemic uncertainty. Understanding the behavior of BO methods under such conditions is crucial for planning appropriate actions. Specifically, we investigated how varying the number of initial samples affects the optimization process to answer the **RQ3**. The analysis was conducted across three environments: Ackley, Alpine, and SynGP, with evaluations performed at three different levels of initial samples (Figure 9). According to Table 3, our results indicate that with fewer initial points, the GP surrogate model struggles to accurately approximate the ground-truth function, thereby increasing the likelihood of suboptimal outcomes across both myopic and nonmyopic methods.

To address this issue, we enhance the diversity of the generated outputs and introduce a warm-up phase for the amortized network parameters during each BO iteration. Specifically, we set the  $\kappa$  concentration hyperparameter of the von Mises–Fisher distribution (distribution of noises added to output) to 0, which promotes a more diverse range of outputs. For the warm-up phase, the amortized network is initialized with randomly generated data points, preventing the generated outputs from being confined to a local region. This approach ensures broader coverage of the receptive field, facilitating better exploration. The refined results are presented in Figure 10, demonstrating the effectiveness of this strategy within the SynGP environment.

### E.3 Varying the Choice of Gaussian Process Kernel

Since our surrogate models are GPs, their quality is influenced not only by the number of data points but also by the choice of kernel. In this section, we address the **RQ3**, focusing on the impact of kernel selection on GP performance. To evaluate this, we tested different kernel functions, including the Radial Basis Function (RBF) kernel and the Matérn kernel with  $\nu = 1.5$ , across three functions: Ackley, Alpine, and SynGP. Figure 11 visualizes the ablation results. Numerical results are presented in Table 4. This ablation demonstrates that with any well-fitted kernel, the nonmyopic approach can achieve the global optimum.

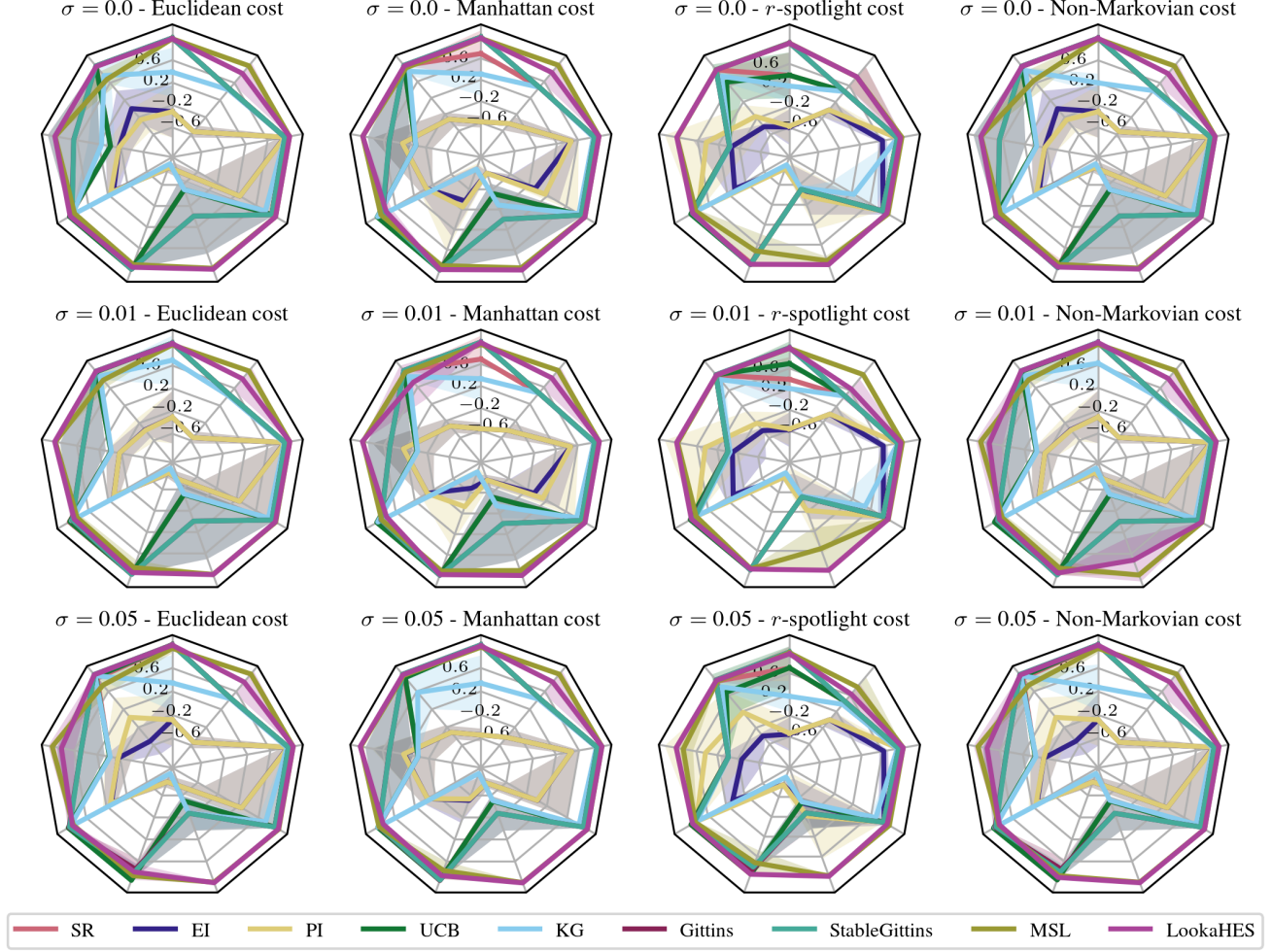


Figure 8: Final observed value. Starting from noon, counter-clockwise: Ackley, Ackley4D, Alpine, Cosine8, Hartmann, HolderTable, Levy, StyblinskiTang, SynGP. We observe that LookaHES consistently achieves the global optimum across various types of cost structures and noise levels.

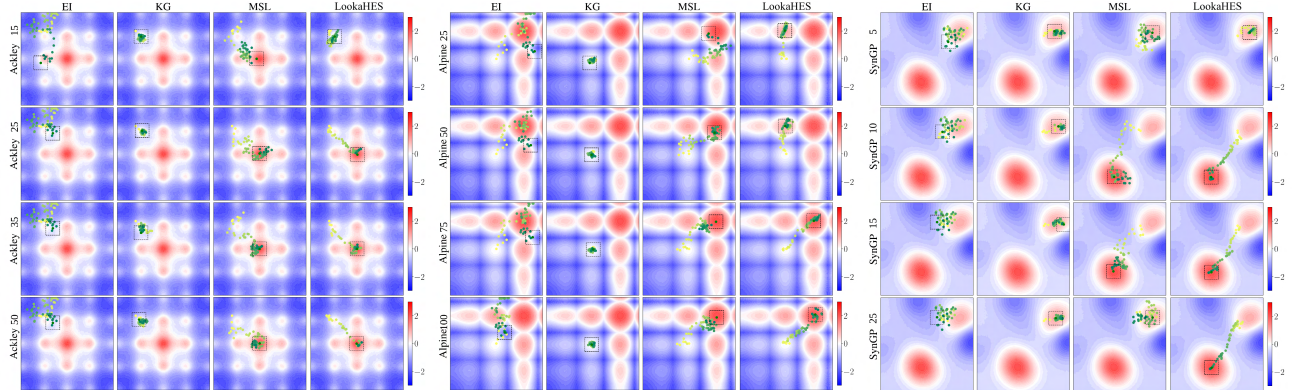


Figure 9: Comparison of performance between LookaHES and baselines with different numbers of initial samples. The yellow points indicate the starting positions, while the green points represent the final actions. From top to bottom, the Ackley function is evaluated with 15, 25, 35, and 50 initial samples; the Alpine function with 25, 50, 75, and 100 initial samples; and the SynGP function with 5, 10, 15, and 25 initial samples. With a small number of initial samples, all methods tend to fail to find the global optimum due to poor surrogate models.

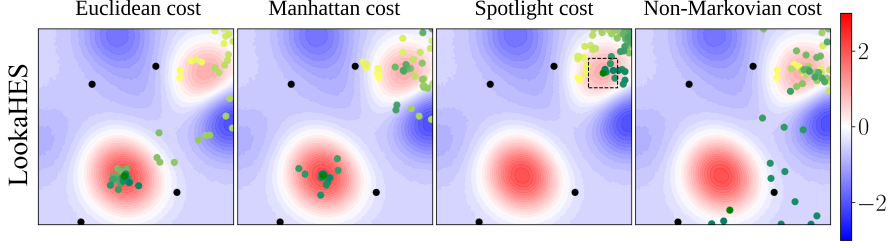


Figure 10: SynGP environment with 5 initial points and our diversity-enhanced BO method. The black points are data. The yellow points indicate the starting positions, while the green points represent the final actions.

Table 3: Comparison of performance between LookaHES and baselines with different numbers of initial samples.

Function	Init Points	EI	KG	MSL	LookaHES
Ackley	15	0.276 $\pm$ 0.490	0.042 $\pm$ 0.051	0.533 $\pm$ 0.283	<b>0.678 <math>\pm</math> 0.402</b>
	25	-0.545 $\pm$ 0.308	0.329 $\pm$ 0.465	<b>0.986 <math>\pm</math> 0.017</b>	0.965 $\pm$ 0.021
	35	-0.540 $\pm$ 0.302	0.328 $\pm$ 0.468	0.943 $\pm$ 0.027	<b>0.991 <math>\pm</math> 0.014</b>
	50	-0.553 $\pm$ 0.317	0.164 $\pm$ 0.289	0.963 $\pm$ 0.034	<b>0.993 <math>\pm</math> 0.013</b>
Alpine	25	-0.174 $\pm$ 0.277	-0.016 $\pm$ 0.008	0.455 $\pm$ 0.355	<b>0.654 <math>\pm</math> 0.237</b>
	50	-0.008 $\pm$ 0.493	-0.047 $\pm$ 0.051	<b>0.915 <math>\pm</math> 0.048</b>	0.571 $\pm$ 0.320
	75	-0.113 $\pm$ 0.400	-0.008 $\pm$ 0.006	<b>0.901 <math>\pm</math> 0.120</b>	0.823 $\pm$ 0.235
	100	-0.271 $\pm$ 0.411	-0.017 $\pm$ 0.012	0.973 $\pm$ 0.014	<b>0.990 <math>\pm</math> 0.005</b>
SynGP	5	0.173 $\pm$ 0.110	0.418 $\pm$ 0.024	0.452 $\pm$ 0.003	<b>0.449 <math>\pm</math> 0.001</b>
	10	0.074 $\pm$ 0.065	0.416 $\pm$ 0.050	0.631 $\pm$ 0.256	<b>0.810 <math>\pm</math> 0.254</b>
	15	-0.001 $\pm$ 0.172	0.401 $\pm$ 0.036	0.804 $\pm$ 0.251	<b>0.808 <math>\pm</math> 0.249</b>
	25	-0.001 $\pm$ 0.172	0.379 $\pm$ 0.054	<b>0.920 <math>\pm</math> 0.100</b>	0.810 $\pm$ 0.255

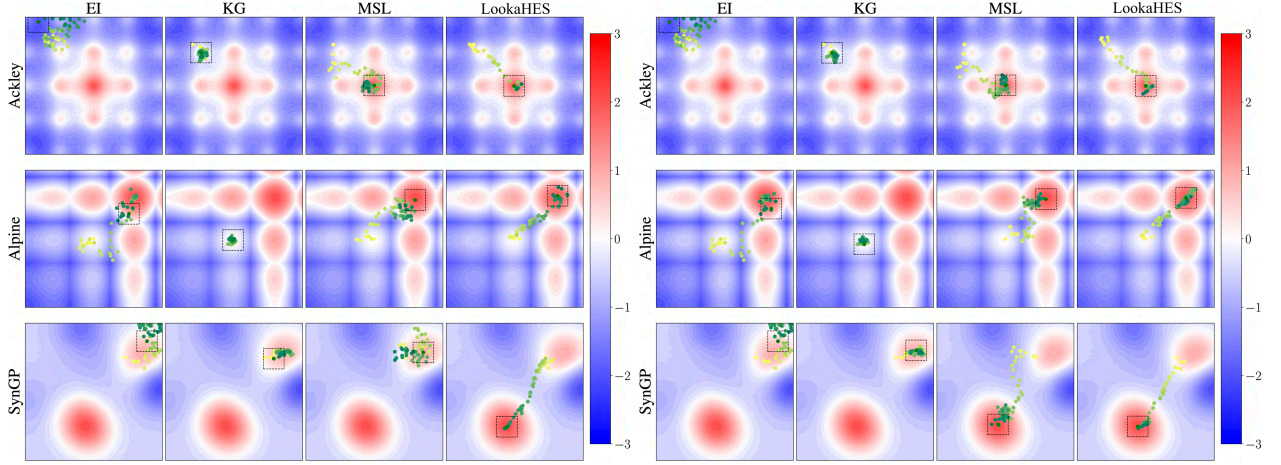


Figure 11: Comparison of performance between LookaHES and baselines with different kernels for the surrogate model (RBF on the left, and Matern on the right). The yellow points indicate the starting positions, while the green points represent the final actions. The performance of LookaHES is not affected by the choice of kernel for the surrogate model as long as the surrogate model can approximate the target function effectively.

In our synthetic experiments, we do not include an ablation study on the Bayesian linear regression model, as it is unsuitable for accurately approximating the non-linear target functions. To demonstrate this limitation, we compared the posterior surface generated by Bayesian linear regression with those of other kernel-based methods, as shown in Figure 12. These results confirmed its inadequacy, leading us to exclude it from our ablation study.

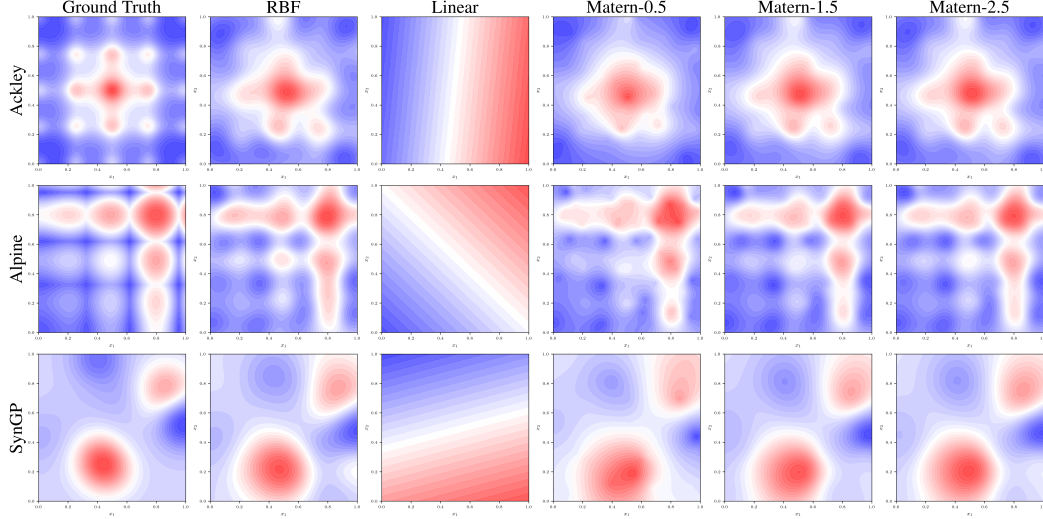


Figure 12: Comparison of posterior surfaces of different kernels on Ackley, Alpine, and SynGP function. Using Bayesian linear regression (the third column) resulted in a wrong approximation of the ground truth functions.

Table 4: Comparison of performance between LookaHES and baselines with different kernels for the surrogate model.

Kernel	Function	EI	KG	MSL	LookaHES
RBF	Ackley	$-0.553 \pm 0.317$	$0.164 \pm 0.289$	$0.963 \pm 0.034$	$0.993 \pm 0.013$
	Alpine	$-0.271 \pm 0.411$	$-0.017 \pm 0.012$	$0.973 \pm 0.014$	$0.990 \pm 0.005$
	SynGP	$-0.001 \pm 0.172$	$0.379 \pm 0.054$	$0.920 \pm 0.100$	$0.810 \pm 0.255$
Matern 0.5	Ackley	$-0.553 \pm 0.317$	$0.215 \pm 0.544$	$0.881 \pm 0.102$	$-0.101 \pm 0.461$
	Alpine	$-0.059 \pm 0.705$	$-0.076 \pm 0.047$	$0.976 \pm 0.009$	$0.317 \pm 0.474$
	SynGP	$-0.001 \pm 0.172$	$0.398 \pm 0.018$	$0.974 \pm 0.003$	$-0.039 \pm 0.349$
Matern 1.5	Ackley	$-0.553 \pm 0.317$	$0.067 \pm 0.049$	$0.969 \pm 0.007$	$0.769 \pm 0.289$
	Alpine	$-0.188 \pm 0.525$	$-0.060 \pm 0.019$	$0.988 \pm 0.005$	$0.823 \pm 0.236$
	SynGP	$-0.001 \pm 0.172$	$0.400 \pm 0.044$	$0.989 \pm 0.003$	$0.630 \pm 0.255$
Matern 2.5	Ackley	$-0.553 \pm 0.317$	$0.067 \pm 0.049$	$0.969 \pm 0.007$	$0.769 \pm 0.289$
	Alpine	$-0.188 \pm 0.525$	$-0.060 \pm 0.019$	$0.988 \pm 0.005$	$0.823 \pm 0.236$
	SynGP	$-0.001 \pm 0.172$	$0.400 \pm 0.044$	$0.989 \pm 0.003$	$0.630 \pm 0.255$

#### E.4 Varying the Length of the Lookahead Horizon

To answer **RQ3** on the benefit of a large lookahead horizon, we included experimental results on the ablation of the number of lookahead steps in Figure 13 and Table 5. These results illustrate the relationship between the number of lookahead steps and the robustness of the optimization, providing insights into how the performance of our approach varies with different horizon lengths. Specifically, with a smaller lookahead horizon, the probability of being trapped by local optima increases, leading to suboptimal optimization in all nonmyopic methods.

The experiments conducted across various scenarios highlight the robustness and effectiveness of our proposed method in handling different challenges in Bayesian optimization. We observed that varying observation noise levels (0%, 1%, and 5%) had minimal impact on the performance of LookaHES compared to baseline approaches, with LookaHES consistently achieving the global optimum across all cost structures and noise settings. Additionally, we found that limited initial samples led to suboptimal performance due to high epistemic uncertainty, but introducing a diversity-enhancing strategy and a warm-up phase improved the results. Kernel selection also played a crucial role, and LookaHES demonstrated strong performance regardless of the kernel choice as long as the surrogate model could approximate the target function effectively. Finally, our results show that incorporating a

larger lookahead horizon significantly improves the optimization process, reducing the likelihood of being trapped in local optima.

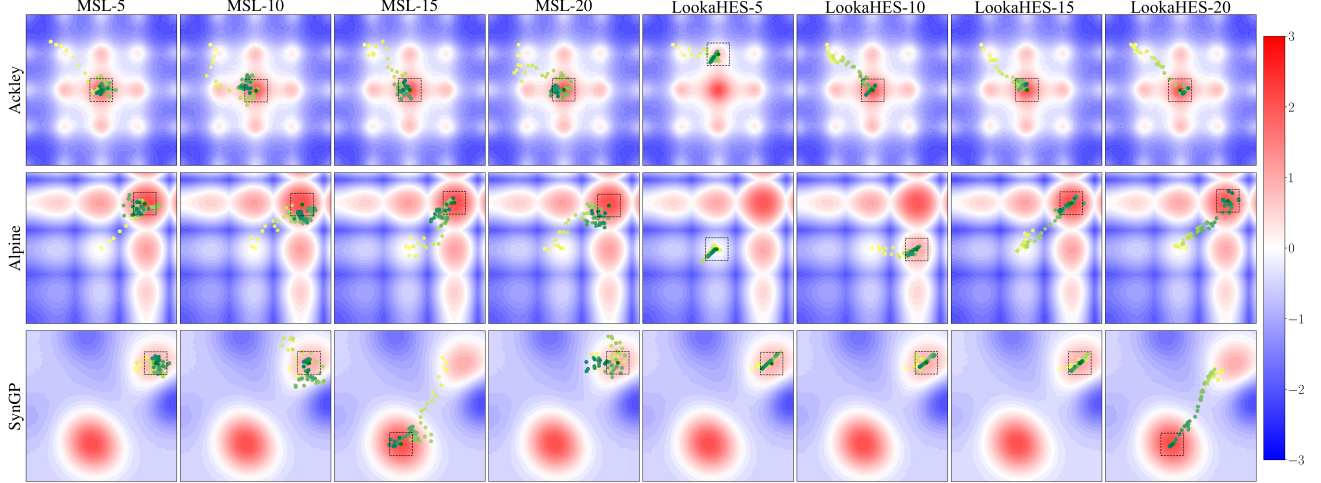


Figure 13: Comparison of LookaHES and nonmyopic baseline at 5, 10, 15, and 20 lookahead steps. The yellow points indicate the starting positions, while the green points represent the final actions. With fewer lookahead steps, nonmyopic methods tend to fail to find the global optimum, demonstrating the benefit of having a longer lookahead horizon.

Table 5: Comparison of LookaHES and nonmyopic baseline at 5, 10, 15, and 20 lookahead steps.

Function	Method	5	10	15	20
Ackley	MSL	0.992 $\pm$ 0.013	0.986 $\pm$ 0.012	0.983 $\pm$ 0.015	0.963 $\pm$ 0.034
	LookaHES	0.979 $\pm$ 0.018	0.991 $\pm$ 0.013	0.995 $\pm$ 0.009	0.993 $\pm$ 0.013
Alpine	MSL	0.983 $\pm$ 0.008	0.987 $\pm$ 0.008	0.947 $\pm$ 0.038	0.973 $\pm$ 0.014
	LookaHES	0.990 $\pm$ 0.006	0.989 $\pm$ 0.005	0.990 $\pm$ 0.006	0.990 $\pm$ 0.005
SynGP	MSL	0.452 $\pm$ 0.003	0.630 $\pm$ 0.253	0.988 $\pm$ 0.004	0.920 $\pm$ 0.100
	LookaHES	0.452 $\pm$ 0.003	0.452 $\pm$ 0.003	0.452 $\pm$ 0.003	0.810 $\pm$ 0.255

**Summary:** Our proposed method demonstrated robustness to aleatoric noise, maintaining strong performance even with a 5% noise level. High epistemic uncertainty from limited initial samples hindered performance, but strategies like diversity enhancement and warm-up phases mitigated this issue. Additionally, effective surrogate model design and a larger lookahead horizon were crucial, enhancing optimization by avoiding local optima and improving convergence.

## E.5 Varying the Acquisition Function Hyperparameters

Myopic acquisition functions, such as UCB, rely on “optimism” during optimization. This means they prioritize exploration with the expectation that querying enough points may eventually uncover the optimum. In this section, we investigate whether this “optimism” can outperform lookahead methods, addressing **RQ4**. In the case of the UCB acquisition function, the degree of optimism is controlled by the  $\beta$  hyperparameter: smaller values of  $\beta$  emphasize exploitation, while larger values encourage exploration. With sufficiently large  $\beta$ , the standard deviation term dominates the mean term, leading to decisions driven by the most uncertain areas. Additionally, the PI acquisition function has a  $\tau$  parameter to control optimism, with smaller values encouraging exploration. To further illustrate the impact of  $\beta$  and  $\tau$ , we conducted additional experiments with  $\beta$  values ranging from 0.1 to 1000,  $\tau$  values ranging from 0.1 to 20 on nine synthetic functions. Other myopic functions, including SR, EI, and KG, do not have a mechanism to handle optimism. In Figure 14, we highlight the behavior of UCB when increasing  $\beta$ .

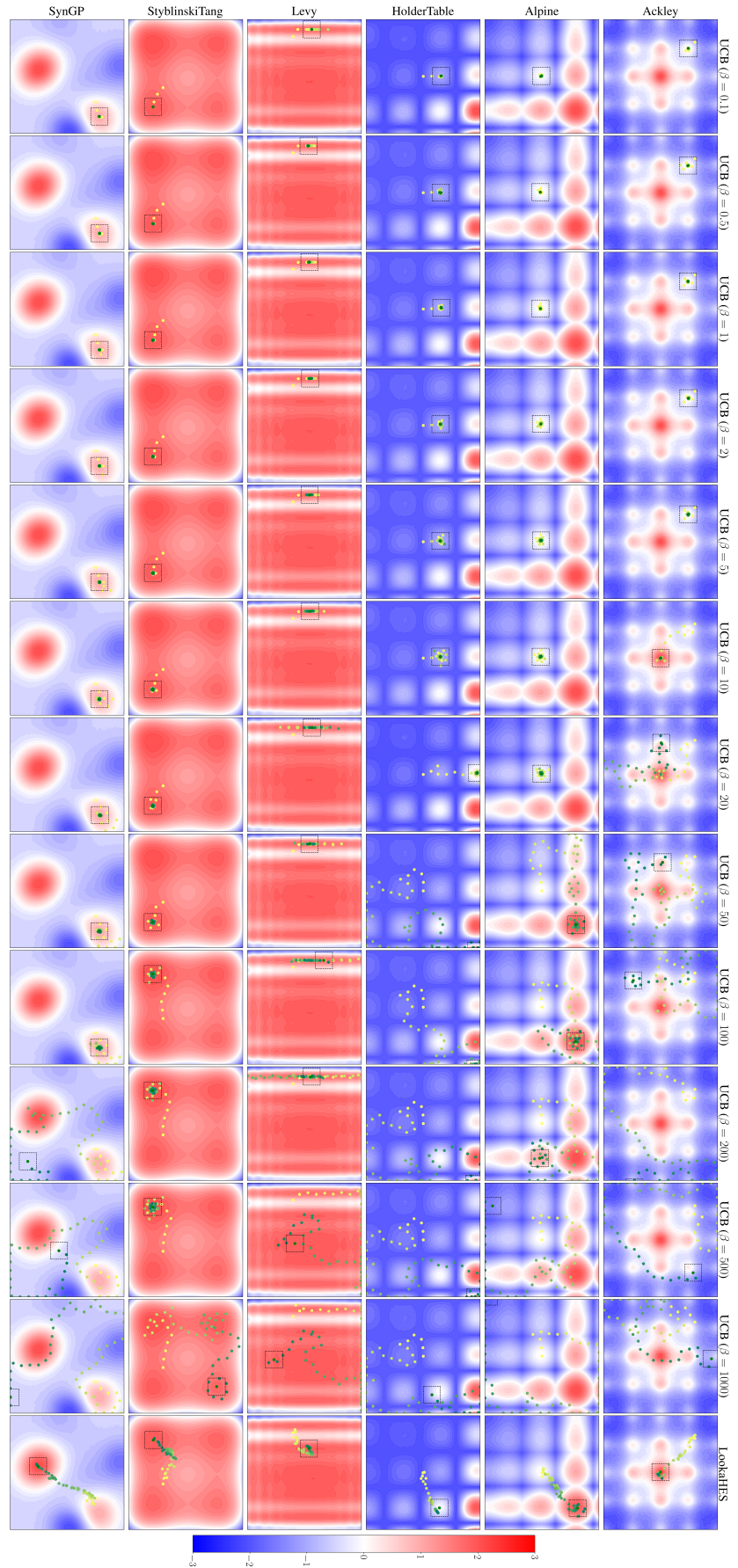


Figure 14: Visualization of queries across BO iterations with the setting of  $\sigma = 0.0$  and r-spotlight cost. The yellow points indicate the starting positions, while the green points represent the final actions. With an appropriate  $\beta$ , the UCB can achieve the global optimum as ours.

We also provide the value of the final action, normalized to range from -1 to 1, where -1 represents the worst outcome and 1 is the best in Table 6. These empirical results further illustrate that the large  $\beta$  value can encourage the decision-maker to make queries that highly prioritize exploration. As illustrated in the above figure and table, such exploration is typically myopic and unplanned, and consequently, the decision maker typically misses the global optima or overexplores the un-promising region. We also want to note that in our experiment, no single  $\beta$  outperformed others in all settings: for example,  $\beta = 10$  works well for Ackley, but does not work for other functions. Indeed, choosing the value of  $\beta$  for UCB before running the online experiment is nontrivial in practice.

Table 6: Comparison of the final action value of LookaHES with 20-step lookahead and UCB with various  $\beta$  values

Method	Ackley	Ackley4D	Alpine	Cosine8	Hartmann	HolderTable	Levy	StyblinskiTang	SynGP
LookaHES	0.99 $\pm$ 0.01	0.97 $\pm$ 0.02	<b>0.99 <math>\pm</math> 0.01</b>	0.93 $\pm$ 0.01	0.96 $\pm$ 0.03	0.05 $\pm$ 0.08	<b>0.95 <math>\pm</math> 0.0</b>	<b>1.0 <math>\pm</math> 0.0</b>	<b>0.81 <math>\pm</math> 0.26</b>
UCB ( $\beta = 0.1$ )	0.7 $\pm$ 0.4	0.68 $\pm$ 0.44	-0.01 $\pm$ 0.01	0.96 $\pm$ 0.01	0.95 $\pm$ 0.02	-0.49 $\pm$ 0.01	0.87 $\pm$ 0.0	0.91 $\pm$ 0.0	0.45 $\pm$ 0.01
UCB ( $\beta = 0.5$ )	0.4 $\pm$ 0.41	0.68 $\pm$ 0.44	-0.01 $\pm$ 0.01	<b>0.97 <math>\pm</math> 0.01</b>	0.94 $\pm$ 0.04	-0.5 $\pm$ 0.01	0.87 $\pm$ 0.0	0.91 $\pm$ 0.0	0.45 $\pm$ 0.01
UCB ( $\beta = 1$ )	0.4 $\pm$ 0.41	0.67 $\pm$ 0.43	-0.01 $\pm$ 0.01	0.96 $\pm$ 0.02	0.95 $\pm$ 0.03	-0.49 $\pm$ 0.01	0.87 $\pm$ 0.0	0.91 $\pm$ 0.0	0.45 $\pm$ 0.01
UCB ( $\beta = 2$ )	0.4 $\pm$ 0.41	0.68 $\pm$ 0.44	-0.01 $\pm$ 0.01	0.97 $\pm$ 0.02	0.95 $\pm$ 0.03	-0.49 $\pm$ 0.01	0.87 $\pm$ 0.0	0.91 $\pm$ 0.0	0.45 $\pm$ 0.01
UCB ( $\beta = 5$ )	0.7 $\pm$ 0.43	0.98 $\pm$ 0.01	-0.01 $\pm$ 0.01	0.96 $\pm$ 0.03	<b>0.97 <math>\pm</math> 0.02</b>	-0.49 $\pm$ 0.01	0.87 $\pm$ 0.0	0.91 $\pm$ 0.0	0.45 $\pm$ 0.01
UCB ( $\beta = 10$ )	<b>1.0 <math>\pm</math> 0.01</b>	0.98 $\pm$ 0.01	-0.01 $\pm$ 0.01	0.97 $\pm$ 0.02	0.96 $\pm$ 0.03	-0.28 $\pm$ 0.32	0.87 $\pm$ 0.0	0.91 $\pm$ 0.0	0.45 $\pm$ 0.01
UCB ( $\beta = 20$ )	0.71 $\pm$ 0.35	0.87 $\pm$ 0.17	0.15 $\pm$ 0.24	0.97 $\pm$ 0.04	0.97 $\pm$ 0.03	-0.03 $\pm$ 0.34	0.87 $\pm$ 0.0	0.91 $\pm$ 0.0	0.45 $\pm$ 0.01
UCB ( $\beta = 50$ )	0.55 $\pm$ 0.65	<b>0.99 <math>\pm</math> 0.01</b>	0.73 $\pm$ 0.36	0.88 $\pm$ 0.04	0.94 $\pm$ 0.03	0.81 $\pm$ 0.6	0.87 $\pm$ 0.0	0.91 $\pm$ 0.0	0.45 $\pm$ 0.01
UCB ( $\beta = 100$ )	0.45 $\pm$ 0.41	0.47 $\pm$ 0.33	0.92 $\pm$ 0.09	0.71 $\pm$ 0.06	0.95 $\pm$ 0.03	0.9 $\pm$ 0.81	0.86 $\pm$ 0.01	0.94 $\pm$ 0.04	0.45 $\pm$ 0.01
UCB ( $\beta = 200$ )	-0.34 $\pm$ 0.38	-0.72 $\pm$ 0.06	0.15 $\pm$ 0.46	0.62 $\pm$ 0.07	0.81 $\pm$ 0.12	<b>0.76 <math>\pm</math> 0.23</b>	0.93 $\pm$ 0.05	0.93 $\pm$ 0.1	0.22 $\pm$ 0.32
UCB ( $\beta = 500$ )	-0.12 $\pm$ 0.13	-0.33 $\pm$ 0.3	-0.43 $\pm$ 0.48	0.13 $\pm$ 0.18	-0.02 $\pm$ 0.61	0.27 $\pm$ 1.1	0.82 $\pm$ 0.12	0.96 $\pm$ 0.06	0.61 $\pm$ 0.53
UCB ( $\beta = 1000$ )	0.06 $\pm$ 0.5	-0.6 $\pm$ 0.24	-0.2 $\pm$ 0.66	-0.18 $\pm$ 0.1	-0.52 $\pm$ 0.43	-0.41 $\pm$ 0.32	0.84 $\pm$ 0.06	0.92 $\pm$ 0.07	0.5 $\pm$ 0.53
PI ( $\tau = 0.1$ )	-0.55 $\pm$ 0.32	-0.40 $\pm$ 0.06	-0.05 $\pm$ 0.72	0.12 $\pm$ 0.25	-0.85 $\pm$ 0.04	-0.23 $\pm$ 0.84	0.45 $\pm$ 0.77	0.72 $\pm$ 0.13	-0.00 $\pm$ 0.17
PI ( $\tau = 0.5$ )	-0.51 $\pm$ 0.27	-0.12 $\pm$ 0.38	0.38 $\pm$ 0.75	0.71 $\pm$ 0.02	-0.85 $\pm$ 0.04	-0.30 $\pm$ 0.74	0.84 $\pm$ 0.02	0.88 $\pm$ 0.02	-0.00 $\pm$ 0.17
PI ( $\tau = 1$ )	0.21 $\pm$ 0.55	0.48 $\pm$ 0.05	-0.13 $\pm$ 0.02	0.93 $\pm$ 0.02	0.87 $\pm$ 0.10	-0.59 $\pm$ 0.07	0.84 $\pm$ 0.02	0.91 $\pm$ 0.00	0.38 $\pm$ 0.04
PI ( $\tau = 2$ )	0.40 $\pm$ 0.41	0.64 $\pm$ 0.42	-0.10 $\pm$ 0.05	0.93 $\pm$ 0.03	0.96 $\pm$ 0.03	-0.60 $\pm$ 0.05	0.87 $\pm$ 0.00	0.91 $\pm$ 0.00	0.45 $\pm$ 0.01
PI ( $\tau = 5$ )	0.70 $\pm$ 0.41	0.66 $\pm$ 0.43	-0.01 $\pm$ 0.01	0.96 $\pm$ 0.01	0.94 $\pm$ 0.04	-0.50 $\pm$ 0.01	0.87 $\pm$ 0.00	0.91 $\pm$ 0.00	0.45 $\pm$ 0.01
PI ( $\tau = 10$ )	0.70 $\pm$ 0.40	0.97 $\pm$ 0.01	-0.01 $\pm$ 0.01	0.96 $\pm$ 0.01	0.94 $\pm$ 0.03	-0.49 $\pm$ 0.01	0.87 $\pm$ 0.00	0.91 $\pm$ 0.00	0.45 $\pm$ 0.01
PI ( $\tau = 20$ )	0.70 $\pm$ 0.40	0.95 $\pm$ 0.05	-0.01 $\pm$ 0.01	0.95 $\pm$ 0.01	0.93 $\pm$ 0.01	-0.49 $\pm$ 0.01	0.87 $\pm$ 0.00	0.91 $\pm$ 0.00	0.45 $\pm$ 0.01

Our experiments demonstrate that while large values of the  $\beta$  hyperparameter in the UCB acquisition function prioritize exploration, they often lead to myopic and unplanned exploration, causing the decision-maker to miss the global optimum or over-explore unpromising regions. The performance of UCB varies across different functions, with no single  $\beta$  value outperforming others universally, highlighting the challenge of selecting an optimal  $\beta$  before running the experiment. This underscores the complexity of using optimism in myopic methods compared to more structured lookahead approaches.

**Summary:** Optimism in myopic methods, such as using a large  $\beta$  in the UCB acquisition function, can lead to unplanned exploration and suboptimal performance, as it risks missing the global optimum or over-exploring unpromising areas. While this optimism may occasionally benefit specific scenarios, its lack of consistency across functions limits its broad applicability to real-world problems compared to more structured, nonmyopic approaches.

## E.6 Synthetic Functions with Discrete Input

In many practical scenarios, data domains exhibit discrete attributes, such as those encountered in natural language processing or chemical molecular structures. To answer the **RQ2** and demonstrate the efficiency of LookaHES within discrete spaces, we conducted an additional experiment. In this experiment, we utilized the SynGP environment. However, in this case, we discretized the domain of each dimension into  $C$  categories, such that the design variable belongs to the set  $\mathbb{C}^d$ , where  $d$  represents the number of design dimensions. The categorical variables are represented in a one-hot encoding format. At time step  $t$ , the design variable  $x_t$  is a matrix of size  $C \times d$ , with  $x_t = [x_t^i]_{i=1}^d$ , where  $x_t^i \in \mathbb{C}$  denotes the one-hot encoded vector for the  $i$ -th dimension.

To adapt our variational network to this discrete domain, we modify its architecture as follows. To compute the representation  $x'_t$  of the design variable for the variational network, each dimension  $x_t^i$  is passed through a linear transformation, followed by a sum-pooling operation across dimensions:  $x'_t = \sum_{i=1}^d W x_t^i$ . The output of the variational network is a probability vector corresponding to a categorical distribution. To ensure gradient

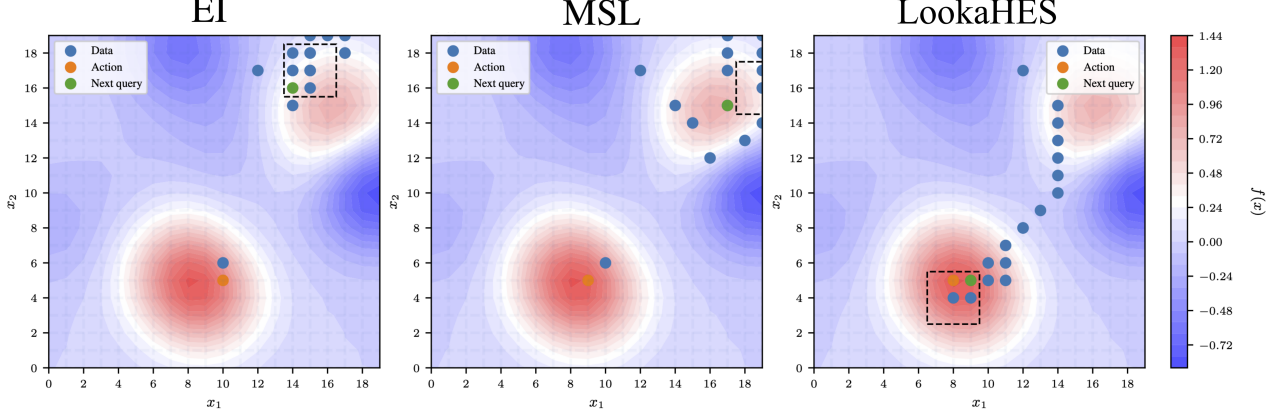


Figure 15: Results of discrete setting on SynGP. From left to right: EI, MSL, LookaHES

propagation during optimization, we sample the most likely category using the Straight-through reparameterization technique [Bengio et al., 2013].

The MSL acquisition function in discrete domains does not benefit from gradient-based optimization methods to minimize the loss function. As a result, MSL is implemented using a multistep combinatorial search in this experiment. This approach significantly increases computational complexity, especially when dealing with a large number of categories. For instance, in the SynGP environment, where an input variable has 20 categories, and the MSL algorithm is configured with  $L = 4$  lookahead steps, the number of combinations to explore is given by  $(C^d)^L = (20^2)^4 = 25.6 \times 10^9$ , leading to an exponentially large search space. Given the constraints of limited computational resources, we resort to a random search with a budget of 2000 possible design variable configurations.

Figure 15 presents a comparative analysis of the performance of the myopic acquisition functions EI, MSL, and our proposed acquisition function within the discrete SynGP after 18 BO iterations. As shown, LookaHES outperforms the other acquisition functions. This experiment thus highlights the robustness of our approach in addressing optimization problems in discrete domains.

### E.7 Ablation of Cost Noises

In the real world, sometimes we can not compute the cost function exactly. In other words, the cost function is only an approximation of real-world cost. We perform ablation studies on the cost functions with 5% noise. The results are presented in Table 7.

Table 7: Comparison of optimization methods across environment and cost function with 5% noise.

Environment	Cost Function	EI	KG	MSL	LookaHES
Ackley	Euclidean	$-0.031 \pm 0.441$	$0.980 \pm 0.003$	$0.966 \pm 0.012$	<b><math>0.998 \pm 0.011</math></b>
	Manhattan	$-0.303 \pm 0.259$	$0.683 \pm 0.437$	$0.966 \pm 0.035$	<b><math>0.993 \pm 0.010</math></b>
	Non-Markovian	$-0.031 \pm 0.441$	$0.982 \pm 0.013$	$0.957 \pm 0.031$	<b><math>0.995 \pm 0.011</math></b>
Alpine	Euclidean	$-0.352 \pm 0.257$	$0.325 \pm 0.476$	<b><math>0.953 \pm 0.027</math></b>	$0.947 \pm 0.055$
	Manhattan	$-0.200 \pm 0.108$	$0.158 \pm 0.236$	$0.964 \pm 0.007$	<b><math>0.990 \pm 0.006</math></b>
	Non-Markovian	$-0.352 \pm 0.257$	$-0.008 \pm 0.006$	$0.954 \pm 0.042$	<b><math>0.990 \pm 0.006</math></b>
SynGP	Euclidean	$-0.349 \pm 0.292$	$0.452 \pm 0.003$	<b><math>0.984 \pm 0.001</math></b>	$0.810 \pm 0.256$
	Manhattan	$-0.243 \pm 0.238$	$0.452 \pm 0.003$	<b><math>0.988 \pm 0.003</math></b>	$0.810 \pm 0.251$
	Non-Markovian	$-0.349 \pm 0.292$	$0.452 \pm 0.003$	$0.988 \pm 0.002$	<b><math>0.989 \pm 0.003</math></b>

## E.8 High-Dimensional Experiments

We further evaluate our method in high-dimensional settings using the Ackley function in 20 and 50 dimensions. For these environments, we consider three representative cost functions: *Euclidean*, *spotlight*, and *non-Markovian*. We exclude the Manhattan cost in high-dimensional experiments, as it is rarely used in such regimes: distances under the  $\ell_1$  metric tend to concentrate as dimensionality increases, rendering them less informative and often leading to degraded performance in Bayesian optimization methods. We also omit Knowledge Gradient from these experiments. In high-dimensional settings, KG becomes computationally intractable and consistently results in out-of-memory errors on an NVIDIA A100 GPU with 80 GB of memory.

Table 8 reports the results across all high-dimensional configurations (20D and 50D). Overall, our method achieves performance that is comparable to, and in several cases matches, the strongest baseline in each setting, across all considered cost functions and dimensionalities. This demonstrates that our approach remains robust and competitive even as the dimensionality of the search space increases substantially.

Table 8: Performance on high-dimensional Ackley function with 5% observation noise under different cost functions

Setting (Function, Cost)	SR	EI	PI	UCB	MSL	LookaHES
Ackley20D, Euclidean	$0.83 \pm 0.04$	$-0.69 \pm 0.00$	$-0.19 \pm 0.40$	$0.83 \pm 0.04$	$0.64 \pm 0.06$	$0.80 \pm 0.05$
Ackley20D, Spotlight	$0.76 \pm 0.02$	$-0.70 \pm 0.09$	$0.01 \pm 0.44$	$0.77 \pm 0.05$	$0.80 \pm 0.01$	$0.89 \pm 0.08$
Ackley20D, Non-Markovian	$0.86 \pm 0.01$	$-0.40 \pm 0.21$	$-0.19 \pm 0.40$	$0.83 \pm 0.04$	$0.64 \pm 0.06$	$0.85 \pm 0.08$
Ackley50D, Euclidean	$0.84 \pm 0.02$	$-0.56 \pm 0.12$	$-0.56 \pm 0.00$	$0.83 \pm 0.03$	$0.43 \pm 0.08$	$0.71 \pm 0.04$
Ackley50D, Spotlight	$-0.27 \pm 0.21$	$-0.72 \pm 0.06$	$-0.79 \pm 0.06$	$-0.11 \pm 0.02$	$0.81 \pm 0.01$	$0.74 \pm 0.03$
Ackley50D, Non-Markovian	$0.83 \pm 0.03$	$-0.57 \pm 0.00$	$-0.61 \pm 0.07$	$0.83 \pm 0.03$	$0.43 \pm 0.08$	$0.57 \pm 0.16$

## F Details of Night Light Experiments

To demonstrate the applicability of LookaHES in real-world continuous environments, we conducted experiments on human travel optimization within a 2D continuous domain. This experiment addresses **RQ1** in the context of continuous domains. Specifically, we used a 2016 grayscale image of night lights in Georgia and South Carolina, sourced from NASA’s Earth Observatory, with a resolution of  $1000 \times 1000$  pixels. The data is online accessible at <https://earthobservatory.nasa.gov/features/NightLights>. To facilitate the optimization of the GP surrogate model and avoid numerical issues due to image noise, we applied a stack blur with a radius of 50 to the image. The pixel values, ranging from 0 to 255, were normalized to a range of  $-3$  to  $3$ . The image width and height were normalized to a range of 0 to 1. We apply LookaHES and baselines with spotlight cost ( $r = 0.1$ ) and Euclidean cost. Figures 16 show the results of LookaHES and baselines on the spotlight and Euclidean cost, respectively. In this environment, nonmyopic methods demonstrated their advantage in lookahead capability. Notably, LookaHES showed its effectiveness in directly reaching the global optimum, rather than querying around sub-optimal locations before approaching the global optimum as MSL. Table 9 presents the numerical results of this experiment with three different seeds.

Table 9: Values of Final Action in The NightLight Environment. All Values Are Scaled To  $(-1, 1)$ .

Cost	SR	EI	PI	UCB	KG	MSL	LookaHES
Spotlight	0.54 $\pm 0.000$	-0.79 $\pm 0.107$	-0.79 $\pm 0.107$	0.54 $\pm 0.000$	0.54 $\pm 0.000$	0.97 $\pm 0.016$	<b>0.99</b> $\pm 0.005$
Euclidean	0.54 $\pm 0.000$	-0.57 $\pm 0.492$	-0.62 $\pm 0.423$	0.54 $\pm 0.000$	0.21 $\pm 0.258$	0.97 $\pm 0.029$	<b>0.99</b> $\pm 0.011$

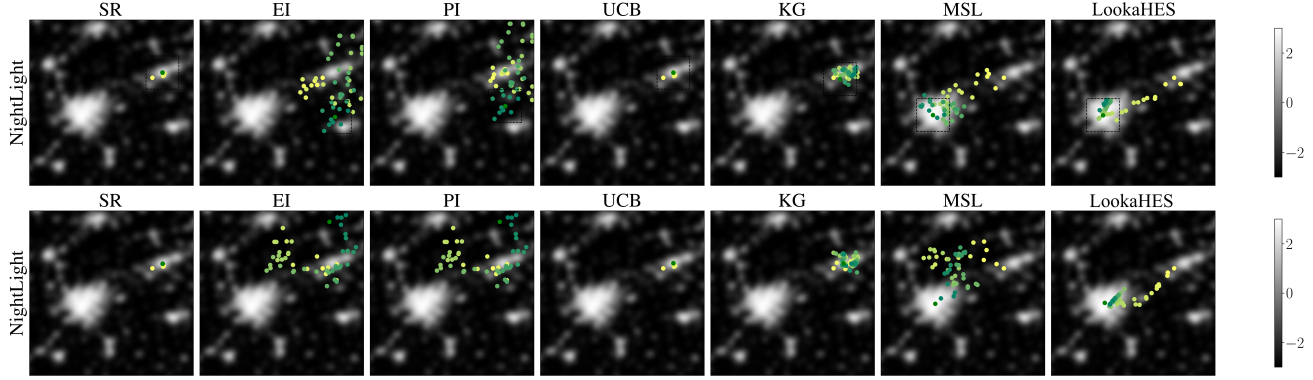


Figure 16: Visualization of different methods on NASA night light images in the case of spotlight cost (top row) and Euclidean cost (bottom row)

## G Details of Protein Sequence Design Experiments

### G.1 Oracle Goodness of Fit

We assess the Oracle model’s performance with increasing training data to gauge how well our semi-synthetic setting approximates real data. The Oracle is a Bayesian linear regression model that takes protein embeddings from various large language models, ranging from Llama-2 7B (a general-purpose model) to ESM-2 3B (a protein-specific model). Our results show that the Gemma 7B embeddings yield the best regression performance, leading us to use Gemma 7B in subsequent experiments.

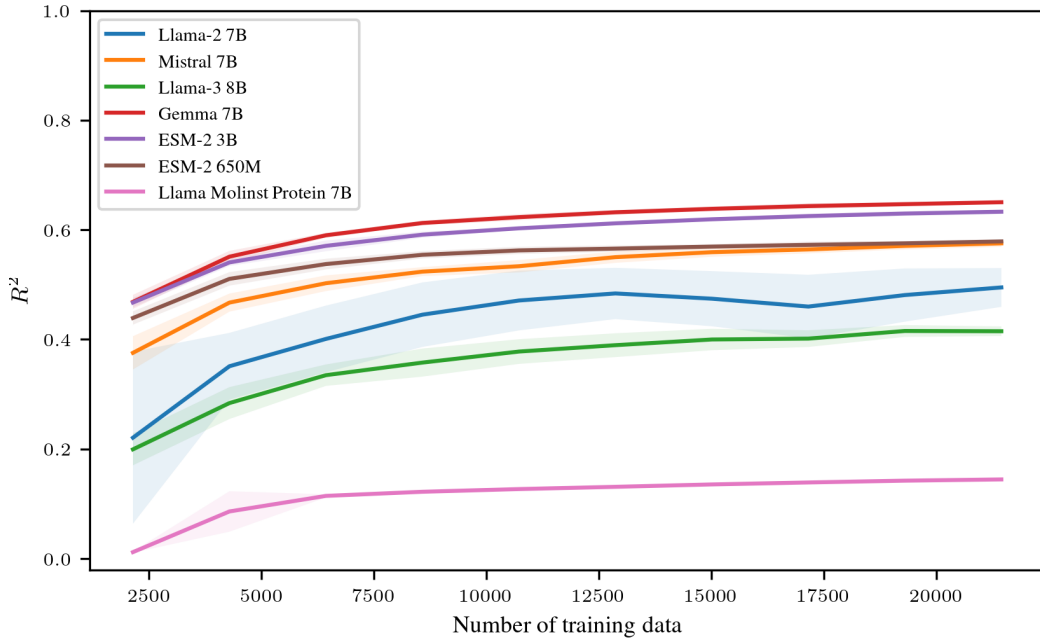


Figure 17: Coefficient of determination on the test set as a function of the number of training data. The  $R^2$  metric is used to evaluate the performance of embedding protein sequences.

### G.2 Modeling Protein Sequence Design with Natural Language

We employ the instruction-finetuned Llama-3.2 3B model as our variational network. The model is available online at <https://huggingface.co/meta-llama/Llama-3.2-3B-Instruct>. We frame the protein design process as a dialogue to leverage the model’s conversational capabilities. Specifically, we prompt the model to generate the

next protein sequences based on previously observed protein and their fluorescent level. The prompts we used are outlined below.

System prompt:

```
You are a helpful assistant who works in a protein engineering lab. We are trying to edit a given protein
→ by a sequence of 1-step protein editing, known as mutation. You need to use your knowledge to
→ help me propose suitable protein editing. Going from an initial protein to an optimal one can
→ take many steps.
```

First prompt:

```
Edit 1 amino acid in the below protein sequence to create a new protein with higher fluorescence. The
→ amino acid must be in set {D, E}. Protein sequence: {starting_protein}
```

Feedback prompt:

```
Fluorescence level of the above protein: {fluorescence_level} Based on the above protein sequence and its
→ fluorescence value, edit 1 amino acid to achieve higher fluorescence. You must only return the
→ modified protein sequence and nothing else. Modified protein sequence:
```

### G.3 Supervised fine-tuning Process

Before starting the BO process, we conduct supervised fine-tuning (SFT) on the variational network to adapt it to the protein design task. We generate a dataset for SFT training consisting of 100 dialogues, each containing  $L$  rounds corresponding to the number of lookahead steps. The proteins in each dialogue are created by either randomly mutating or retaining the previous protein. The fine-tuning hyperparameters are provided below.

Table 10: SFT Hyperparameters

Hyperparameter	Value
Learning rate	$10^{-4}$
Epochs	3.3
Batch size	4
Learning rate warmup ratio	0.1
Learning rate schedule	Cosine
LoRA $\alpha$	32
LoRA $r$	16
LoRA dropout	0.1
LoRA target modules	q-proj, v-proj

### G.4 Nonmyopic Bayesian Optimization as Multi-turn Proximal Policy Optimization

Proximal Policy Optimization (PPO) [Schulman et al., 2017] is typically used to fine-tune language models for single-turn conversations, where the model responds once to a prompt without considering future turns. However, our approach requires the model to think ahead and generate multiple future queries (in this case, protein sequences) over several turns. To address this, we modify existing PPO frameworks to handle multturn conversations, allowing the model to generate and optimize future sequences during training. We also use vLLM [Kwon et al., 2023], a system designed to improve the speed and efficiency of inference (i.e., generating outputs from the model). However, vLLM is an inference engine and cannot be used directly for training [Kwon et al., 2023]. To overcome this, after each step of updating the model during training (called a gradient step), we transfer the updated model’s weights (parameters) to the vLLM system. This allows us to use vLLM for faster generation of outputs, leading to more efficient training. Additionally, running vLLM with PPO simultaneously on multiple GPUs is challenging for large language models due to differences in how vLLM and PPO handle GPU VRAM. To address this, we employ Ray [Moritz et al., 2018] to isolate the GPU environments for vLLM and PPO, creating a pipeline that enables efficient weight synchronization between them. Figure 18 illustrates the process of weight syncing between PPO and vLLM.

In the PPO training process, we calculate a final reward for each dialogue using a function  $\ell$ . This function varies depending on the acquisition method being used (e.g., expected improvement or simple regret). Once the

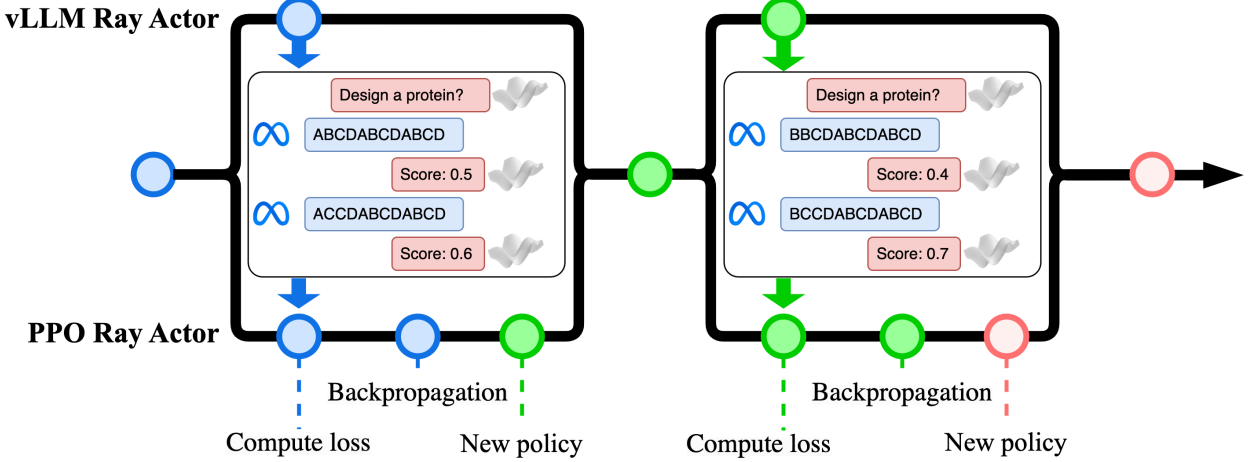


Figure 18: The designed PPO pipeline with vLLM using Ray involves the vLLM actor generating multi-turn protein refinements and calling a surrogate model to compute reward scores. These scores, along with the generated data, are passed to the PPO actor to compute loss, backpropagate, and update the LLM weights. The updated weights from the PPO actor are then synced to the vLLM actor for the next generation.

reward is computed, it is adjusted, or “discounted,” for each individual turn in the dialogue. This means that actions taken earlier in the conversation get less reward compared to later actions. We then use this discounted reward as feedback to update the model during PPO training. By doing this, we extend the single-turn PPO framework, which normally handles one response at a time, to work for our multturn conversation data. The hyperparameters used for fine-tuning PPO are provided below.

Table 11: PPO and Rollout Hyperparameters

Hyperparameter	Value
Learning rate	$10^{-4}$
Epochs	64
Batch size	1
Learning rate warmup ratio	0.1
Learning rate schedule	Cosine
LoRA $\alpha$	256
LoRA $r$	128
LoRA dropout	0.1
LoRA target modules	q-proj, v-proj
Maximal rollout retry	32
Discount reward factor	0.95

## H Ablation Study on Protein Design Experiments

We conduct an ablation study using two different starting proteins and two distinct synthetic functions  $g(x)$  to construct diverse protein spaces, enabling a systematic analysis of their characteristics. The two synthetic functions are defined as follows:

$$g_1(x) = -0.005(d - 0.5)(d - 5)(d - 8)(d - 13.4),$$

$$g_2(x) = -e^{-0.7\sqrt{0.5 \cdot d^2}} - e^{0.5 \cdot \cos(0.4\pi d)} + e + 0.3. \quad (3)$$

Here,  $g_1(x)$  represents a polynomial function that introduces one local maxima across the input space, while  $g_2(x)$  is a more complex one with two local maxima. Visualizations of the resulting protein spaces, derived from the combination of starting proteins and synthetic functions, are shown in Figure 19.

Table 12: Protein Space Constraints

No.	Starting protein	Allowed positions	posi-	Allowed AAs
#1	SKGEELFTGVVPILVELGGDVNGHKFSVSGEGEGDATYGKLT KFICTTGKLPVPWPTLVTTLSYGVQCFSRFPDHMKQHDFFKSA MPEGYVQERTIFSKDDGNYKTRAEVKFEGDELVNRIELKGIDF KEEENILGHKLEENYNSHNVYIMADDQKNGIKVNFKIRHNIED DSVQLADHYQQNTPIGDEPVLLPDDHYLSTQSALSKDDNEDRD EMVLLEFVTAAGITHGMDELYK	116, 131, 132, 141, 154, 171, 172, 189, 196, 209, 212, 215		
#2	SKPEELFTPVVGILVELDPDVNGHKFSVSGEGEPDATYGKLT KFICTTGKLGVGWGLTTLVTTLSYGVQCFSRYPDHMKQHDFFKSA MPEGYVQERTIFFKDDGNYKTRAEVKFEPDTLVNRIELKGIVF KEDGNTLGHKLEYNNYNSHNVYIMADEQKNGIKVNFKIRHNIED GSVQLADHYQQNTPIPDGPVLLPDNHYLSTQSALSKDPNEKRD HMVLLEFVTAAGITHGMDELYK	2, 8, 11, 18, 33, 52, 54, 56, 114, 158, 187, 190		G, P

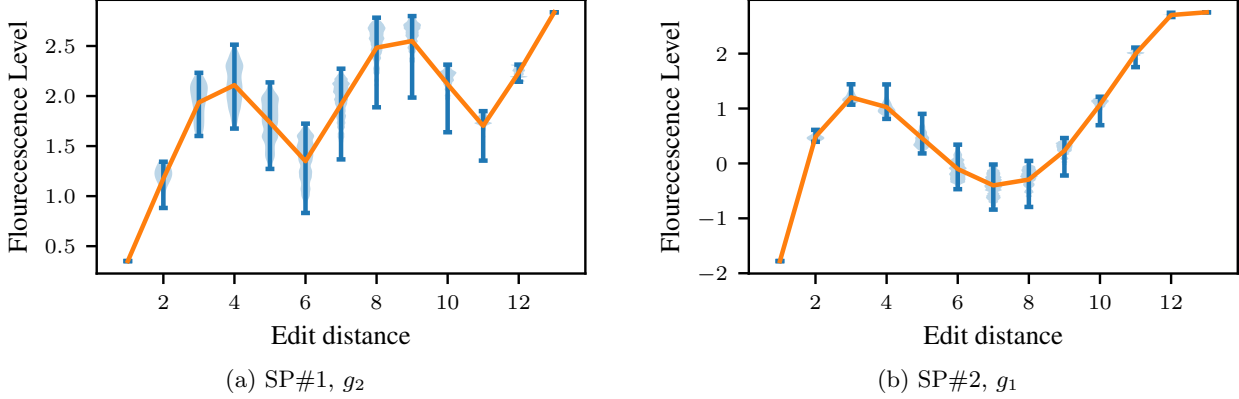


Figure 19: Ablation of protein spaces with varying starting proteins and synthetic functions

We present the results of additional experiments on protein design with the same starting protein with  $g_2$  (Figure 20 top), and with a different starting protein with  $g_1$  (Figure 20 bottom). These figures demonstrate that our proposed nonmyopic method outperforms other myopic baselines in various settings regardless of different starting proteins or synthetic value functions.

We visualize the designed proteins in the experiments of starting protein #1 and  $g_1$ . We use ESM-Fold [Lin et al., 2022] to fold the designed proteins and PyMol [Schrödinger, LLC, 2015] to visualize them. The visualizations are presented in Table 13.

## I Impact Statement

This work presents a novel method for nonmyopic BO in dynamic cost settings, utilizing neural network policies to address long-horizon sequential decision-making. The proposed algorithm is computationally efficient and improves decision-making under uncertainty, with applications in complex scenarios like protein sequence design. Ethical implications include applications in healthcare (e.g., personalized treatment plans) and education (e.g., adaptive learning technologies), where effective and equitable resource allocation is critical. Mitigating biases and ensuring transparency will be essential to prevent systemic inequalities. This research advances machine learning for complex decision-making while emphasizing fairness and ongoing evaluation to ensure ethical deployment.

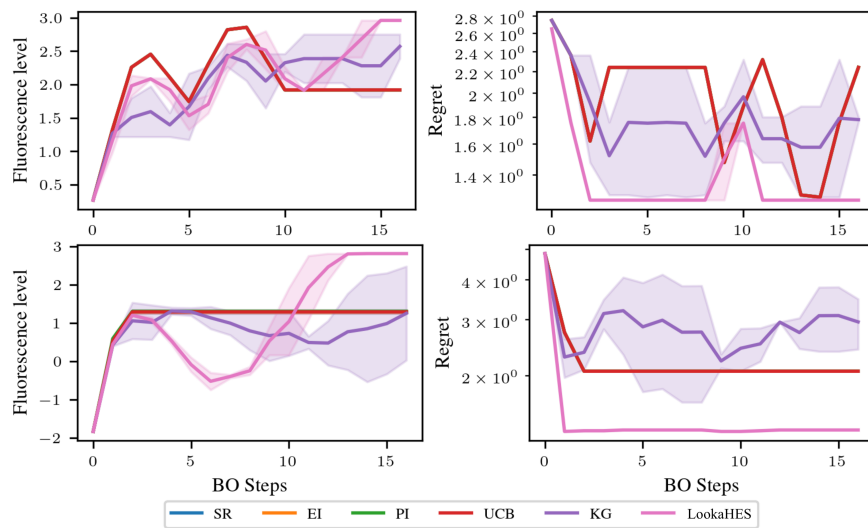


Figure 20: Fluorescence levels (left) and regret (right) observed over Bayesian Optimization (BO) steps. The top row shows results for experiments starting with protein #1 and function  $g_2$ , while the bottom row corresponds to experiments starting with protein #2 and function  $g_1$ .

Table 13: Visualization of Designed Proteins. Edited Amino Acids Are Highlighted in Red.

Sequence	3D Structure
<b>Starting protein:</b> SKGEELFTGVVPILVELGGDVNGHKFSVSSEG EGDATYGKLTGKFICTTGKLPVPWPTLVTTLSYGVQCFSRFPDHKMQH DFFKSAMPEGYVQERTIFSKDDGNYKTRAEVKFEGDELNRIELKGID FKKEENILGHKLEENYNSHNVYIMADDQKNGIKVNFKIRHNIEDDSVQ LADHYQQNTPIGDEPVLLPDDHYLSTQSALKDDNEDRDEMVLLEFVT AAGITHGMDELYK	
<b>LookaHES - Optimal:</b> SKGEELFTGVVPILVELGGDVNGHKFS VSGEGEGDATYGKLTGKFICTTGKLPVPWPTLVTTLSYGVQCFSRFPD HMKQHDFFKSAMPEGYVQERTIFSKDDGNYKTRAEVKFEGDDLVNRIE LKGIDFKEDDNILGHKLEDNYNSHNVYIMADEQKNGIKVNFKIRHNIE EESVQLADHYQQNTPIGDDPVLLPDEHYLSTQSALKDENEERDDMVL LEFVTAAGITHGMDELYK	
<b>SR:</b> SKGEELFTGVVPILVELGGDVNGHKFSVSSEGEGDATYGKLTG FICTTGKLPVPWPTLVTTLSYGVQCFSRFPDHKMQHDFFKSAMPEGYV QERTIFSKDDGNYKTRAEVKFEGDELNRIELKGIDFKEEDNILGHKL EENYNSHNVYIMADDQKNGIKVNFKIRHNIEDDSVQLADHYQQNTPIG DDPVLLPDDHYLSTQSALKDDNEDRDEMVLLEFVTAAAGITHGMDELY K	
<b>EI, PI, UCB:</b> SKGEELFTGVVPILVELGGDVNGHKFSVSSEGEGD ATYGKLTGKFICTTGKLPVPWPTLVTTLSYGVQCFSRFPDHKMQHDF KSAMPEGYVQERTIFSKDDGNYKTRAEVKFEGDELNRIELKGIDFKE DENILGHKLEENYNSHNVYIMADDQKNGIKVNFKIRHNIEDDSVQLAD HYQQNTPIGDEPVLLPDDHYLSTQSALKDENEERDEMVLLEFVTAA GITHGMDELYK	
<b>KG:</b> SKGEELFTGVVPILVELGGDVNGHKFSVSSEGEGDATYGKLTG FICTTGKLPVPWPTLVTTLSYGVQCFSRFPDHKMQHDFFKSAMPEGYV QERTIFSKDDGNYKTRAEVKFEGDELNRIELKGIDFKEEENILGHKL EENYNSHNVYIMADDQKNGIKVNFKIRHNIEDDSVQLADHYQQNTPIG DEPVLLPDDHYLSTQSALKDDNEERDEMVLLEFVTAAAGITHGMDELY K	